



Permafrost Thawing and Estimates of Vulnerable Carbon in the Northern High Latitude

Imran Nadeem^{1,2} · Nebojsa Nakicenovic³ · Asma Yaqub¹ · Boris Sakschewski⁴ · Sina Loriani⁴ · Govindasamy Bala⁵ · Thejna Tharammal⁶ · Caroline Zimm³

Received: 10 May 2024 / Revised: 27 September 2024 / Accepted: 1 October 2024
© The Author(s) 2024

Abstract

The degradation of permafrost in the Northern Hemisphere is expected to persist and potentially worsen as the climate continues to warm. Thawing permafrost results in the decomposition of organic matter frozen in the ground, which stores large amounts of soil organic carbon (SOC), leading to carbon being emitted into the atmosphere in the form of carbon dioxide and methane. This process could potentially contribute to positive feedback between global climate change and permafrost carbon emissions. Accurate projections of permafrost thawing are key to improving our estimates of the global carbon budget and future climate change. Using data from the latest generation of climate models (CMIP6), this paper explores the challenges involved in assessing the annual active layer thickness (ALT), defined as the maximum annual thaw depth of permafrost, and estimated carbon released under various Shared Socioeconomic Pathway (SSP) scenarios (SSP1-2.6, SSP2-4.5, SSP3-7.0 and SSP5-8.5). We find that the ALT estimates derived from CMIP6 model soil temperatures show significant deviations from the observed ALT values. This could lead to inconsistent estimates of carbon release under climate change. We propose a simplified approach to improve the estimate of the changes in ALT under future climate projections. These predicted ALT changes, combined with present-day observations, are used to estimate vulnerable carbon under future climate projections. CMIP6 models project ALT changes of 0.1–0.3 m per degree rise in local temperature, resulting in an average deepening of approx. 1.2–2.1 m in the northern high latitudes under different scenarios. With increasing temperatures, permafrost thawing starts in Southern Siberia, Northern Canada, and Alaska, progressively extending towards the North Pole by the end of the century under high emissions scenarios (SSP5-8.5). Using projections of ALT changes and vertically resolved SOC data, we estimate the ensemble mean of decomposable carbon stocks in thawed permafrost to be approximately 115 GtC (gigatons of carbon in the form of CO₂ and CH₄) under SSP1-2.6, 180 GtC under SSP2-4.5, 260 GtC under SSP3-7.0, and 300 GtC under SSP5-8.5 by the end of the century.

Keywords Permafrost thawing · Climate change · Global warming · Permafrost degradation · Carbon release

1 Introduction

Permafrost, defined as ground that remains frozen (with a temperature less than 0 °C) for an extended period, typically for at least two years, covers nearly a quarter of the Northern Hemisphere land region (Zhang et al. 2005). This expansive permafrost terrain spans diverse environments, from high-latitude Arctic regions, including Siberia, Canada, Alaska, and Greenland, to high-latitude mountainous areas (Zhang et al. 2008). Subsea permafrost is also found beneath the seafloor of the Arctic Sea (Miesner et al. 2023). As a crucial component of the cryosphere, permafrost plays a central role

in regulating climate, hydrology, and ecosystem processes, making it of paramount importance in climate change analyses due to its sensitivity to, and potentially positive feedback mechanisms with, climate change.

The Earth's rising temperatures, observed since the early twentieth century and projected to continue under scenarios of unmitigated emissions, are driving climate trends reminiscent of conditions last witnessed during the Eocene era (Burke et al. 2018). With the global increase in surface temperatures, the extent of permafrost is undergoing a notable reduction, reflecting the shrinking of this frozen ground across various regions worldwide, a direct consequence of escalating surface temperature trends (Lawrence and Slater 2005; Zhang et al. 2005). Over the last decade (2011–2020),

Extended author information available on the last page of the article

the global average surface temperature was 1.09 °C higher than the pre-industrial average (1850–1900), with temperatures in high latitudes rising twice as fast as the global average (Masson-Delmotte et al. 2021). A recent study (Rantanen et al. 2022) indicates that the observed average surface temperature in the Arctic has been increasing almost four times faster than the global average in the last few decades. This phenomenon is termed Arctic amplification, defined as the ratio of high-latitude temperature change to global mean surface temperature change (Koven et al. 2015). The magnitude of changes in Arctic temperatures closely aligns with the changes observed in permafrost, emphasizing the amplification effect and raising significant concerns regarding permafrost degradation and its potential consequences.

Over millions of years, organic carbon has accumulated and been stored in permafrost. The Arctic alone is estimated to contain almost 1400–1600 gigatons of organic carbon (GtC), nearly twice the amount present in the atmosphere (Hugelius et al. 2014; Natali et al. 2021; Schuur et al. 2022). This permafrost, however, is highly unstable and can release greenhouse gases—carbon dioxide (CO₂) and methane (CH₄)—relatively quickly upon thawing (Schuur et al. 2015; Zimov et al. 2006). Permafrost thawing can occur gradually, with a slower warming of permafrost over an extended period, or abruptly, characterized by accelerated thawing over a much shorter timeframe. In a recent study by Nitzbon et al. (2024), the authors underscored that overall response of permafrost to climate change is expected to be gradual, irrespective of global warming levels, similar to the retreat of other cryosphere components. They emphasized that local processes like thermokarst and thermo-erosion can cause rapid permafrost loss, but these changes are region-specific and not globally interconnected, occurring at different times and warming levels. Despite the irreversible nature of carbon loss, there is no evidence for a global-scale climate tipping point for permafrost loss by the end of this century. However, Turetsky et al. (2020) estimate that abrupt permafrost thawing could release 60–100 GtC by 2300, in addition to the 200 GtC from gradual thawing. This abrupt thawing, occurring in less than 20% of permafrost land, significantly increases carbon release projections due to deeper disruptions and higher methane emissions, potentially doubling the climate impacts expected compared to current models.

The interaction between emitted greenhouse gases and consequent heat gain can create a positive feedback loop that intensifies atmospheric and soil warming, accelerating permafrost thawing (Zimov et al. 2006). This raises concerns that permafrost thawing, along with associated temperature rises due to this self-perpetuating positive feedback

mechanism, may become a major tipping element,¹ resulting in significant, irreversible, and policy-relevant impacts (Armstrong McKay et al. 2022; Braghieri et al. 2023; Turetsky et al. 2019). These consequences could profoundly impact both the environment and human societies. By 2050, an estimated three-quarters of the population in the Northern Hemisphere permafrost area could be affected by infrastructural damage caused by permafrost thawing (Hjort et al. 2018).

Modeling studies estimate that the annual mean frozen volume in the permafrost region could decrease by 10–40% with every additional °C increase in global surface air temperature (Burke et al. 2020). The ALT of the permafrost region is predicted to increase by the end of this century, leading to increased vulnerability of permafrost carbon. The spatial variation of permafrost can be characterized by mean annual air temperature (MAAT) and the annual maximum thickness of the thawed layer or ALT. For example, Chadburn et al. (2017) derived a MAAT-permafrost relationship using a robust approach that integrates the spatial distribution of permafrost from an existing map of permafrost in the Northern Hemisphere. In a more recent study, Steinert et al. (2024) presented 10 definitions of permafrost presence, which also include the definition by Chadburn et al. (2017), used for the calculation of permafrost area in climate models. The active layer above permafrost undergoes seasonal thawing and freezing and depends on mean annual air temperature as well as soil properties (Harp et al. 2016). Ground with higher ice content thaws faster than areas with less ice, resulting in a difference in the spatial pattern of ALT.

The Coupled Model Intercomparison Project Phase 6 (CMIP6) is the latest international coupled model comparison program sponsored by the World Climate Research Program (WCRP; Eyring et al. 2016). Similar to the previous phase of the Intercomparison project (CMIP5), the CMIP6 models lack representation of permafrost-carbon-related processes. Underground parameters such as soil temperature profile are also not well simulated by CMIP6 models (Burke et al. 2020). Chadburn et al. (2015) also identified significant issues with the representation of permafrost in most CMIP5 models simulations. These models frequently either misrepresented or entirely omitted permafrost, leading to substantial differences between simulated and observed frozen land areas. The primary cause of these discrepancies was attributed to land-surface dynamics rather than the driving climate. CMIP5 models demonstrated considerable variation in simulating present-day permafrost extent and in their sensitivity to global temperature increases (Koven et al. 2013; Guo and Wang 2016). These inconsistencies

¹ Tipping element is described as a subsystem of the earth system, which may alter quantitatively and irreversibly, if a certain critical threshold called the “tipping point” is passed (Lenton et al. 2008).

were partly due to biases in air temperature and snow depth, but predominantly stemmed from structural weaknesses in land models that limit their ability to simulate subsurface processes in cold regions (Hermoso de Mendoza et al. 2020). Furthermore, most models used in CMIP5 and CMIP6 have bottom boundary conditions in Land Surface Models (LSMs) set at shallow depths between 3 and 10 m, with few exceptions, complicating accurate permafrost representation (Steinert et al. 2021).

Due to the lack of representation of permafrost processes in the climate models, permafrost changes are typically estimated via indirect approaches. Traditional practice is to estimate permafrost thaw based on ALT, which in turn is calculated based on changes in subsurface soil temperatures. Future changes in the active layer have been simulated by previous studies (e.g., Li et al. 2022) based on the CMIP6 temperature data, which simulated spatial and temporal changes in ALT in the Northern Hemisphere. The ability to simulate thaw depths has not improved much between the CMIP5 and CMIP6 model ensembles, due to limitations caused by shallow and poorly resolved soil profiles (Burke et al. 2020). To estimate changes in permafrost carbon, past studies have utilized simplified models of permafrost carbon cycle dynamics, such as the Permafrost Carbon Network Incubation-Panarctic Thermal (PInc-PanTher) scaling approach by Koven et al. (2015). The PInc-PanTher approach used climate anomalies from the CCSM4 climate model (Koven et al. 2013) to force various ecosystem model simulations to simulate soil temperatures, which were then used to estimate the carbon released over the twenty-first century based on carbon rates derived from incubation experiments. While the use of a single model (CCSM4) has provided valuable insights, there is a need to estimate the full spread of future permafrost thaw and associated decomposable carbon under different future emission scenarios. This study aims to address this research gap by using projections from multiple CMIP6 models for a more comprehensive estimation of vulnerable carbon in thawing permafrost under different scenarios. Simulating soil temperatures for ALT estimation using multiple terrestrial biosphere models, each forced with a set of global models, is computationally demanding. Therefore, we employ an alternative method to calculate ALT from surface air temperature projections provided by CMIP6 models. We describe the preparation of bias-corrected ALT, which is used to estimate future changes in permafrost by the end of the century. ALT is estimated based on outputs from multiple models, accounting for the full range of uncertainties arising from different simulated temperatures across the models. Initial estimates of the carbon present in thawed permafrost for various scenarios are calculated based on projected future changes in ALT. This study presents a simple yet effective method, which can be further refined in future research, to

estimate decomposable carbon in thawing permafrost under various emission scenarios.

2 Data Used in the Study

For this study, we utilize data from both CMIP5 and CMIP6. The CMIP5 simulations were based on the representative concentration pathways (RCPs; Meinshausen et al. 2011 and Taylor et al. 2012), which are the concentration pathways used by climate models to project climate change. However, the latest CMIP6 simulations are based on scenarios which combine the latest SSPs (shared socioeconomic pathways; O'Neill et al. 2016) representing socioeconomic and energy-emissions land use scenarios, and updated RCPs. This study uses the most widely used scenarios, namely SSP1-26, SSP2-45, SSP3-70 and SSP5-85. The historical data ranges from the years 1950–2014, whereas the future data range is 2015–2100. The historical and future quantifications were retrieved for a subset of coupled models from CMIP6 model archive, based on availability of data for the scenarios considered. The monthly mean surface air temperature (2-m temperature) and vertically resolved soil temperatures at each soil layer for latitudes poleward of 35°N are used. The CMIP6 models used in this study are shown in Table 1.

For observational data, the “ESA (European Space Agency) Permafrost Climate Change Initiative (Permafrost_CCI): Permafrost active layer thickness for the Northern Hemisphere, v3.0” dataset (Obu et al. 2021) containing permafrost active layer thickness data is used. It is derived from a thermal model driven and constrained by satellite data. The data provides maximum depth of seasonal thaw, which corresponds to the active layer thickness. In the present study, we define the permafrost domain based on this observational dataset, ensuring our analysis focuses on the regions where permafrost is observed according to the ESA Permafrost_CCI data.

The ALT values calculated in this study are compared with the results from the permafrost-enabled dynamic global vegetation model LPJmL (Schaphoff et al. 2018a, b), which was forced with four CMIP5 models.

2.1 LPJmL model

The process-based dynamic global vegetation model (DGVM) LPJmL simulates global vegetation distribution, carbon and water fluxes and stocks, as well as the surface energy balance for natural and managed land ecosystems (Schaphoff et al. 2018a, b). It represents global vegetation with 11 different plant functional types (PFTs) for natural vegetation and 12 crop functional types (CFTs) for agricultural activities. Simulation of plant productivity is based on leaf-level photosynthesis determined by environmental

Table 1 Overview of CMIP6 models used in this study

No	CMIP6 Global Climate Model	Country	Resolution (lon × lat) in degrees
1	ACCESS-CM2	Australia	1.9° × 1.3°
2	ACCESS-ESM1-5	Australia	1.9° × 1.2°
3	BCC-CM2-MR	China	1.1° × 1.1°
4	CAMS-CSMI-0	China	1.1° × 1.1°
5	CanESM5	Canada	2.8° × 2.8°
6	CAS-ESM2-0	China	1.4° × 1.4°
7	CESM2	USA	1.3° × 0.9°
8	CESM2-WACCM	USA	1.3° × 0.9°
9	CMCC-CM2-SR5	Italy	1.3° × 0.9°
10	CMCC-ESM2	Italy	1.3° × 0.9°
11	CNRM-CM6-1	France	0.5° × 0.5°
12	CNRM-CM6-1-HR	France	1.4° × 1.4°
13	CNRM-ESM2-1	France	1.4° × 1.4°
14	EC-Earth3	Europe	0.7° × 0.7°
15	EC-Earth3-Veg-LR	Europe	1.1° × 1.1°
16	EC-Earth3-Veg	Europe	0.7° × 0.7°
17	FGOALS-f3-L	China	1.3° × 1.0°
18	FGOALS-g3	China	2.0° × 2.0°
19	GFDL-CM4	USA	1.0° × 1.25°
20	GFDL-ESM4	USA	1.0° × 1.0°
21	GISS-E2-1-G	USA	2.5° × 2.0°
22	HadGEM3-GC31-LL	UK	1.9° × 1.3°
23	HadGEM3-GC31-MM	UK	0.8° × 0.6°
24	IPSL-CM6A-LR	France	2.5° × 1.3°
25	KACE-1-0-G	South Korea	1.9° × 1.3°
26	MIROC6	Japan	1.4° × 1.4°
27	MIROC-ES2L	Japan	2.8° × 2.8°
28	MPI-ESM1-2-HR	Germany	0.9° × 0.9°
29	MPI-ESM1-2-LR	Germany	1.9° × 1.9°
30	MRI-ESM2-0	Japan	1.1° × 1.1°
31	NorESM2-LM	Norway	2.5° × 1.9°
32	NorESM2-MM	Norway	1.3° × 0.9°
33	TaiESM1	Taiwan	2.5° × 1.9°
34	UKESM1-0-LL	UK	1.9° × 1.3°

conditions (e.g., climate, soil water content or atmospheric CO₂ concentration), and other dynamic variables like canopy conductance, autotrophic respiration, and phenology, as well as variables related to human management. The PFT distribution is influenced by PFT competition, bioclimatic limits and effects of heat and fire. Specific land-use inputs determine CFT distributions and management. For this study LPJmL operates on a grid of 0.5° × 0.5° latitude–longitude with input data of daily air temperature, precipitation, long-wave and shortwave downward radiation, annual atmospheric CO₂ and information on land use and general soil texture. Soil texture data is taken from the Harmonized World Soil Database (HWSD) version 1 (Nachtergaele et al. 2010)

and relationships between texture and hydraulic properties from Cosby et al. (1984). The model simulates soil thermodynamics using a finite-difference approach to solve the heat conduction equation. It includes considerations for freezing and thawing, with thermal properties computed based on soil composition. The model divides the soil column into five hydrologically active layers and an additional thermal buffer layer, totalling 13 m in depth. This detailed layering helps simulate key soil processes affecting temperature and moisture dynamics.

2.2 Spin-up, Transient, and Constant Climate Simulations

Transient simulations with LPJmL model are preceded with a spin-up simulation for 5,000 years starting from bare ground without land-use to equilibrate to pre-industrial PFT distributions and carbon pools (Schaphoff et al. 2018b). To do this, climate input of 1861–1890 was randomly shuffled while keeping atmospheric CO₂ at the 1861 level of 286 ppm. A second adjacent spin-up phase of 400 years shuffling the same climate input then introduces historical land-use input taken from (Fader et al. 2010).

Transient simulations start in the year 1861 while applying historic land-use input (Fader et al. 2010) until the year 2005. After 2005, land use was kept constant. This allows us to understand the effect of climate change in isolation from the possible effects of future land-use change scenarios (Fader et al. 2010). Climate variables used to force LPJmL are modelled by the four CMIP5 (Taylor et al. 2012) models HadGEM2-ES, GFDL-GSM2M, IPSL-CM5A-LR and MIROC5 under RCP8.5 (Riahi et al. 2011) similar to the protocol of the ISIMIP2b model intercomparison project (Warszawski et al. 2014). The bias correction of climate data is described in Frieler et al. (2017) and Lange (2018); atmospheric CO₂ follows the trajectory of RCP8.5 (Riahi et al. 2011).

3 Methodology

3.1 Calculation of ALT Using Soil Temperatures

In this study, we first calculate ALT using monthly mean soil temperature from CMIP6 models. The monthly mean thaw depth (in metres) is defined as depth of the deepest level in the soil column of a given grid cell, at a given month, with soil temperature at or above freezing (0°C), or simply, depth of the lower edge of the deepest thawed layer (Lawrence and Slater 2005). A grid cell is identified as containing permafrost if the maximum ALT (in metres) is shallower than either 3 m or the deepest model soil level for models with

soil depth less than 3 m. This approach gives the value of ‘near surface’ permafrost (Koven et al. 2013).

While a few models with deeper soil profiles reasonably capture summer thaw depth (Burke et al. 2020), limitations in representing water phase changes, such as neglecting the latent heat of freezing/thawing, likely lead to inaccuracies in many other models (Ekici et al. 2014; Burke et al. 2020). Furthermore, increasing LSM depth influences the soil’s ability to store and transfer heat, which in turn can lead to variability in ALT estimates, depending on how specific thermal processes are handled in each model (González-Rouco et al. 2021).

An overestimation or underestimation of ALT can lead to inaccurate projection of carbon release when estimations are derived based on changes in ALT in future decades. It is essential to address this issue before determining how vulnerable carbon stocks are. To accurately determine the permafrost’s physical state, we calculated bias-adjusted ALT with a method developed from the approach of Burke et al. (2013), which estimates the permafrost thawing for each model based on local temperatures.

3.2 Calculation of bias-corrected ALT

At a large scale, the presence of permafrost is predominantly controlled by the MAAT (Chadburn et al. 2017). As neither CMIP5 nor CMIP6 models (Burke et al. 2013) include permafrost-carbon feedback, the physical state of the permafrost has to be quantified from bias-adjusted ALT.

Our method (modified from Burke et al. 2013) reconstructs the ALT time series of the twenty-first century for each grid point, by sampling ALT sensitivity from the 5th–95th percentile range and combining it with the local annual mean near-surface air temperature change for each CMIP6 model. This bias-adjustment method estimates ALT independent of the model soil layers and depths, representing the full spread of uncertainties of the CMIP6 models (similar to simulated air temperatures). The estimated ALT are based on anomalies in air temperature from 34 coupled models participating in CMIP6.

The following steps are then used to calculate active layer sensitivity ($ALT_{\text{sensitivity}}$) to MAAT:

- Soil temperatures from CMIP6 models were interpolated vertically with steps of 0.05 m (5 cm) to minimise the error in estimated ALT. This results in generation of large amounts of data but better estimation of ALT as a poorly resolved soil model introduces biases in the estimate of the ALT (Burke et al. 2012).
- For each model and scenario, ALT is calculated for each year based on interpolated monthly data.
- Using the calculated ALT and MAAT from the CMIP6 models, a relationship between ALT and MAAT is

derived by applying a regression model at each grid box for the period 2015–2100. Only ALT up to 3 m is used for this relationship.

- At each grid point, the regression model is used to estimate the change in ALT per degree change in MAAT. This is called $ALT_{\text{sensitivity}}$.

ALT time series are then reproduced for each grid by combining the previously calculated ALT with $ALT_{\text{sensitivity}}$ based on local mean near-surface air temperature change (Burke et al. 2013). The equation used for reconstruction of the ALT time series is:

$$ALT_{\text{max}}(t, x, y) = ALT_{\text{max}}(t - 1, x, y) + ALT_{\text{sensitivity}}[T_{\theta}(t, x, y) - T_{\text{local}}(t - 1, x, y)] \quad (1)$$

where $ALT_{\text{max}}(t = 0, x, y) = ALTb_{\text{max}}(x, y)$.

Here T_{local} is the local air temperature, t is the time, and x, y identifies each grid cell that has permafrost. The base $ALTb_{\text{max}}$ is the maximum ALT for the period 2011–2015 calculated from the observational data.

The 5th and 95th percentiles of the spatial distribution of $ALT_{\text{sensitivity}}$ to local MAAT are shown in Appendix Table 5. The missing data is marked with blank boxes since some models do not have data available for all SSPs. For the calculation of bias-adjusted ALT, we consider only parameters based on the ensemble mean of all SSP simulations for the period 2015–2100. These are the ensemble mean $ALT_{\text{sensitivity}}$ values (averaged over the Northern Hemisphere Permafrost grid cells) of 5th percentile, median and 95th percentiles. The respective values of these parameters are 0.02, 0.11 and 0.28 m°C respectively (Table 2). These values are very close to the values estimated by Burke et al. (2013) for CMIP5 models, which is another indicator that permafrost physics in the land surface model of CMIP6 models has not changed much since the previous model generation (CMIP5). As the reconstruction of ALT is based on historical observations, the permafrost area calculated from bias-adjusted ALT is the same for all models. The three estimates of twenty-first century ALTmax are combined with the observed distribution of soil organic carbon content to provide estimates of the permafrost climate response. In the next step, 3D profiles of carbon stocks up to 10 m are constructed based on historical carbon stock maps of upper 3-m soils and the total carbon estimations at different depths found in recent literature (Hugelius et al. 2013, 2014; Strauss et al. 2017).

3.3 Carbon Stock Estimates

To estimate the carbon vulnerable to decomposition in future thawing of permafrost, it is important to know the spatial

Table 2 Different percentiles of ensemble mean ALT sensitivity to mean annual air temperature. The values marked in bold are selected for this study

ALT sensitivity	Hist (m/K)	SSP126 (m/K)	SSP245 (m/K)	SSP370 (m/K)	SSP585 (m/K)	All (Hist + SSPs) (m/K)	Only SSPs (m/K)
Mean	0.097	0.105	0.127	0.128	0.123	0.114	0.120
01st Percentile	0.011	0.011	0.011	0.011	0.011	0.011	0.011
05th Percentile	0.017	0.017	0.018	0.017	0.017	0.017	0.017
10th Percentile	0.024	0.023	0.025	0.022	0.022	0.024	0.023
25th Percentile	0.044	0.045	0.050	0.054	0.053	0.047	0.049
Median	0.079	0.085	0.111	0.121	0.116	0.097	0.105
75th Percentile	0.132	0.144	0.183	0.182	0.175	0.161	0.171
90th Percentile	0.191	0.208	0.251	0.238	0.228	0.224	0.233
95th Percentile	0.239	0.261	0.301	0.285	0.266	0.272	0.280
99th Percentile	0.352	0.376	0.412	0.381	0.364	0.380	0.388

Table 3 Permafrost soil organic carbon storage in north circumpolar region, at given soil depth ranges according to different studies, applied in the present study

References	SOC (GtC)	Depth (m)	Methodology
Hugelius et al. (2014)	~472	0–1 m	Updated estimates of SOC in the North Circumpolar Permafrost region, based on different databases and methodologies
	~355	1–2 m	
	~207	2–3 m	
Strauss et al. (2017)	~492	3–10 m	Revised estimates based on different databases and methodologies leading to updated estimates in Permafrost region SOC stocks

distribution of present-day soil organic carbon (SOC) stocks in the permafrost. For depths of up to 3 m below the ground surface, spatial distribution data of SOC is already available from Hugelius et al. (2014), whereas for depths below 3 m, SOC estimates from Strauss et al. (2017) are used, as summarized in Table 3. The spatial distribution of SOC for the first 3 m is illustrated in Appendix Fig. 12 (in Appendix).

Our projections indicate that the ALT will not exceed 10 m by the end of the century, therefore, we can reasonably assume that the SOC at a depth of 10 m is zero. A quadratic regression model is fitted to the known values: 472 GtC for the top layer (0–1 m), 355 GtC for the second layer (1–2 m), 207 GtC for the third layer (2–3 m), and 0 GtC at the 10-m depth, with the constraint that the sum of the carbon stocks from 3 to 10 m equals 492 GtC. The regression model ensures that the total SOC at each depth remains consistent with the known values in Table 3. The interpolated carbon values at 1-m intervals are provided in Table 4. The quadratic function, which provides total carbon at a given depth, is finally employed to interpolate SOC values at finer vertical resolutions, specifically at 5 cm intervals, from the surface to a depth of 10 m.

To spatially distribute the total estimated carbon in 5 cm layers, it is assumed that the horizontal distribution

Table 4 Estimation of Total Carbon at different soil depth ranges calculated in this study for northern circumpolar permafrost region

Depth below ground (m)	Carbon per m (GtC)	Accum. Carbon (GtC)
0–1	472	472
1–2	355	827
2–3	207	1034
3–4	123	1157
4–5	105	1262
5–6	88	1350
6–7	70	1420
7–8	53	1473
8–9	35	1508
9–10	18	1526

patterns of the 0–1 m, 1–2 m, and 2–3 m layers can be applied to their respective sub-layers. For deeper layers, the spatial horizontal distribution observed in the 2–3 m layer is extended. The ratio of SOC in each grid cell of these layers to the total SOC in the Northern Hemisphere for the layer is calculated. These ratios are then used to distribute the total SOC estimates for each 5 cm interval

up to a depth of 10 m. This detailed vertical profile of SOC maintains the consistency of the total SOC at given depths, as shown in Table 4.

While Table 4 provides values at 1-m intervals to give readers a sense of total SOC distribution at these depths, the actual estimation of vulnerable carbon in thawing permafrost is based on data interpolated at a 5 cm vertical resolution. This approach ensures a more precise estimation of carbon vulnerability at finer scales necessary to understand the vulnerability of permafrost carbon stocks in the context of future climate change. Using the calculated SOC estimates over the northern circumpolar permafrost region, we calculate amount of carbon vulnerable to release from thawing permafrost under future climate scenarios.

Finally, the accumulated SOC at each depth is calculated, using the SOC values at 5 cm vertical resolution. This accumulation represents the estimated SOC between the surface and the specific depth. Utilizing these accumulated SOC values, we calculated the amount of vulnerable carbon in thawed permafrost by assessing the change in ALT over different time intervals, such as on a decadal scale.

4 Results

As temperature is a primary driver of permafrost dynamics, understanding regional temperature changes is essential. Figure 1 depicts projected temperature anomalies for global, Arctic, and permafrost regions from 1981 to 2100 under various emission scenarios based on ensemble means of CMIP6 models (Table 1). As already discussed in the introduction, the Arctic exhibits three- to fourfold more warming than the global average, a phenomenon known as Arctic amplification. This directly impacts permafrost regions, where rising temperatures can accelerate thawing, potentially releasing large amounts of greenhouse gases and influencing global climate feedback. As mentioned in Sect. 3(a), initially we compared the ALT calculated from soil temperatures simulated by CMIP6 models with ESA Permafrost_CCI data. The results show over-estimation relative to observations for the historical period (Appendix A, Figs. 13, 14, 15, 16, 17). Because of the inclusion of different land surface models, some of them with insufficient vertical resolution and a limited number of discrete layers for representing subsurface soil profiles, the CMIP6 models show differences in ALT when compared to the observations. Even models with deeper soils are not suitable for ALT calculations (Burke

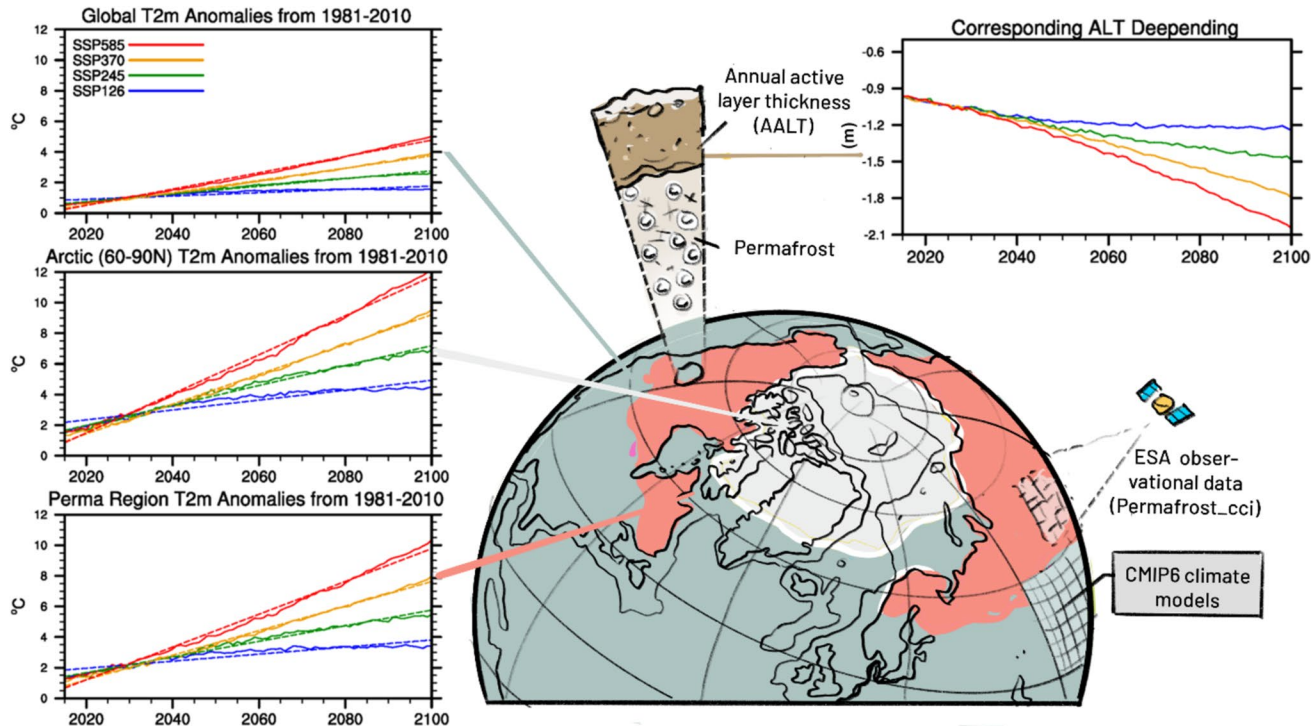


Fig. 1 Arctic amplification: Comparison of surface temperature (at 2 m) anomalies for the permafrost region, high latitudes, and global average from the reference period 1981–2010 based on ensemble

mean of CMIP6 models used in this study. Average deepening of ALT for permafrost regions under various emissions scenarios is also shown

et al. 2020). These values of estimated ALT are not useful for estimating permafrost thawing and corresponding estimations of vulnerable carbon in thawing permafrost. Therefore, we focused our analysis on bias-corrected ALT. Given the full range (5–95%) of ALT sensitivity, we begin our analysis by comparing bias-adjusted ALT with simulated ALT from the LPJmL model. This comparison serves two purposes: (a) to determine whether the estimations of bias-adjusted ALT are comparable to the simulated ALT, and (b) to validate that the median value of ALT sensitivity is closest to the simulated ALT.

As mentioned in Sect. 2, the $ALT_{sensitivity}$ has not changed significantly between the two generations of global models used in CMIP5 and CMIP6. For comparison, we use mean $ALT_{sensitivity}$ values based on CMIP6-based simulations and local temperature from CMIP5 models for calculating bias-adjusted ALT. The CMIP5 model temperature is used because the available LPJmL simulation output was based on CMIP5 forcings. The Fig. 2 shows the LPJmL-simulated average ALT (solid lines) with bias-adjusted ALT (dotted lines) reconstructed from local temperatures using Eq. 1 based on median values of $ALT_{sensitivity}$. Although one of the four models, GFDL-ES2M (Dunne et al. 2012), shows some differences between the LPJmL-simulated and reconstructed ALT, overall year-to-year variations and magnitude of LPJmL-simulated ALT is well represented by bias-adjusted

ALT. The ensemble mean of four models is also included in the comparison. During the mid-century, three of the four models, the exception being IPSL, show a difference of 0.2–0.4 m for mean Northern Hemisphere ALT, but these differences diminish by the last decade of the century. This is also evident when we compare both ALTs representing ensemble means, showing a difference of less than 0.1 m by the end of the century. As Fig. 2 only shows the average ALT for the Northern Hemisphere, it is important to compare bias-adjusted ALT with simulated ALT spatially to see if there are regions with significant differences.

Figure 3 shows the spatial comparison of CMIP6 based on ALT, LPJmL simulated ALT and bias-adjusted ALT calculated from local temperatures for IPSL-CM6A-LR. As already discussed in the previous section and shown in Appendix A, ALT calculated from CMIP6 output shows large overestimation compared to observations. The IPSL-CM6A-LR (Boucher et al. 2020) used for spatial comparison is one of the models with more than 10 m of soil depth. However, the rapid summer thaw of permafrost in such models is likely due to the inadequate representation of the latent heat of the water phase transition, rather than solely the depth of the soil layers. This misrepresentation of phase change dynamics results in an inaccurate calculation of ALT (Burke et al. 2020), leading to unreliable projections. However, the LPJmL model does not

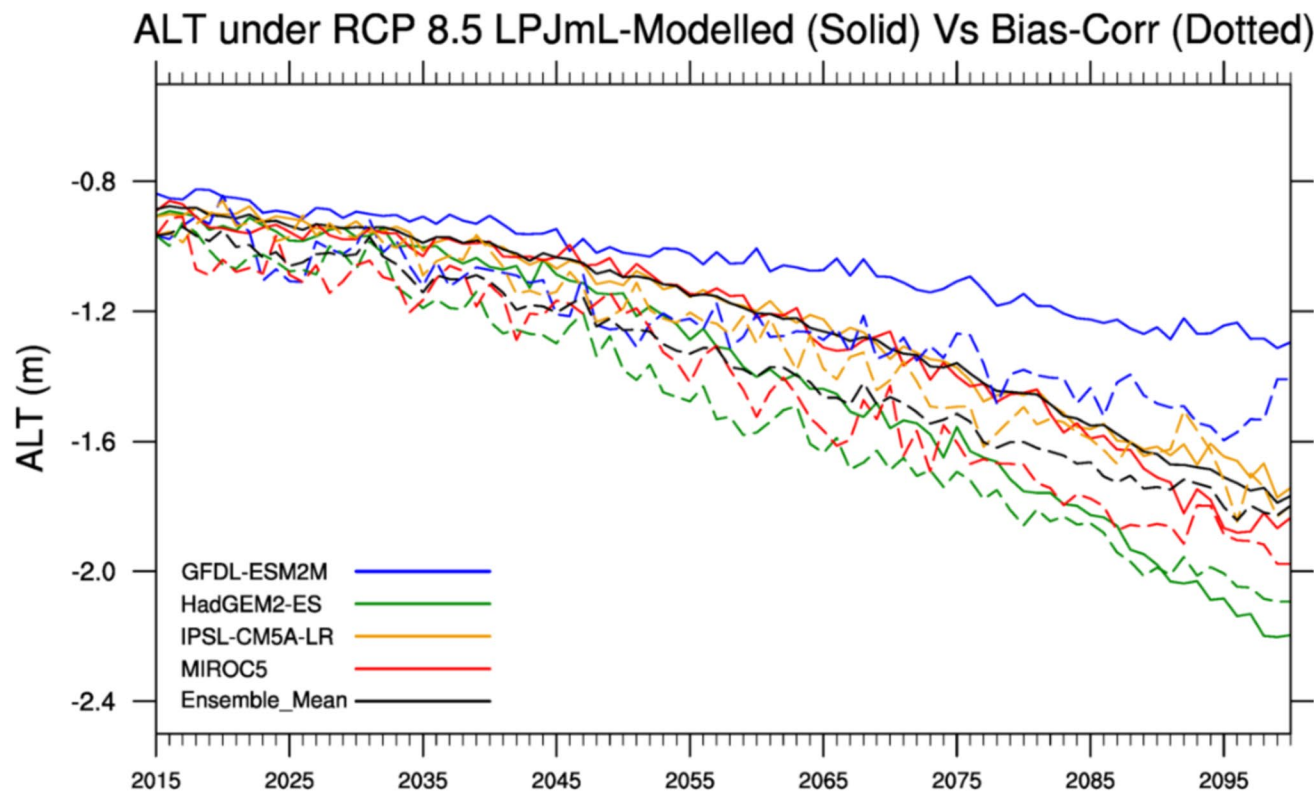


Fig. 2 ALT under RCP 8.5 LPJmL-Modelled (Solid) Vs Bias-adjusted (Dotted)

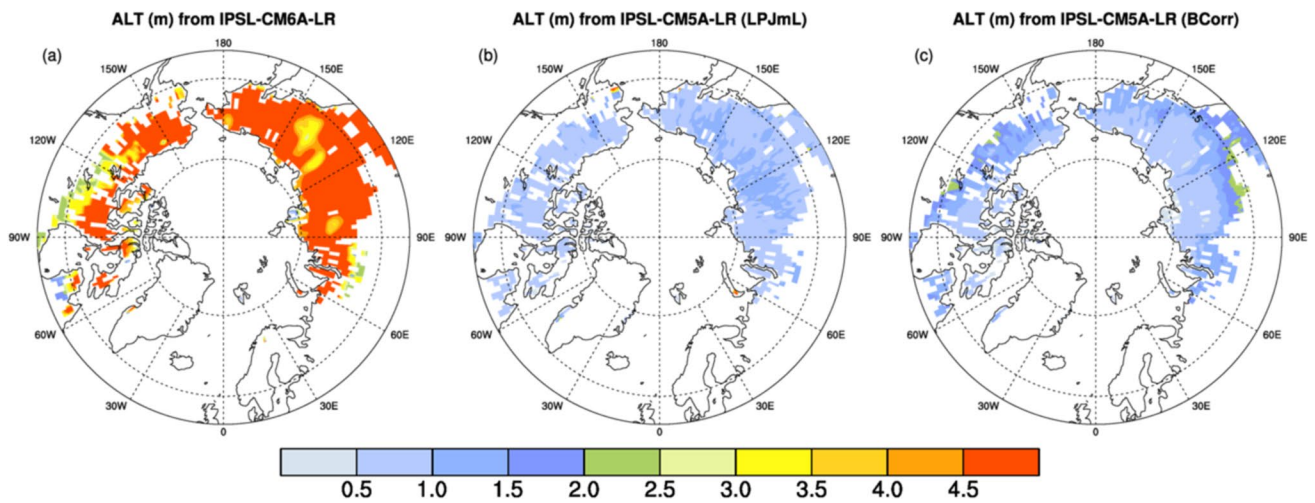


Fig. 3 Spatial comparison of CMIP6 based ALT (a), LPJmL Simulated ALT (b) and Bias-adjusted ALT (c) using median value of $ALT_{sensitivity}$. The ALT values shown here are maximum of the period 2015–2019

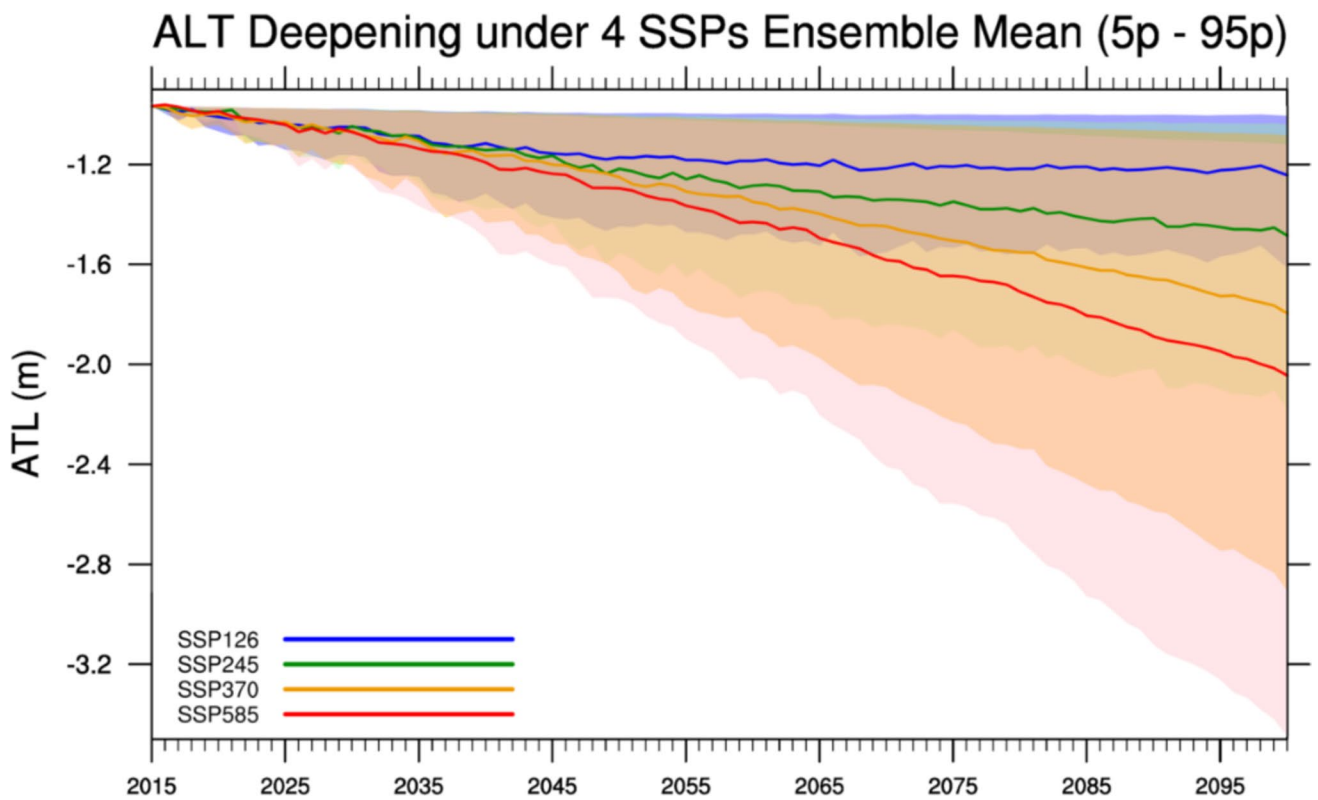


Fig. 4 Mean ALT of the permafrost area for the years 2015–2100. The shaded area represents the spread in ALT when 5th and 95th percentiles of $ALT_{sensitivity}$ are used while solid lines represent the median based ALT values for the Northern Hemisphere permafrost region

overestimate the simulated ALT (Fig. 3b). Figure 3c shows that the ALT estimated from local temperature using median value of $ALT_{sensitivity}$ is slightly overestimated over the Central Siberian Plateau and some regions of Canada, but in general there is good spatial agreement. As simulating ALT using a dynamic global vegetation model like

LPJmL using input data from several coupled climate models and four scenarios requires enormous efforts and computational resources, bias-adjusted ALT with median value of $ALT_{sensitivity}$ is potentially an attractive alternative to LPJmL-simulated ALT for estimation of ALT changes

in the twenty-first century and estimation of CO₂ and/or CH₄ release under different emission scenarios.

The mean Northern Hemisphere ALT reconstructed from local temperature based on 5th percentile, median and 95th percentile value of ALT_{sensitivity} is shown in Fig. 4. At present, the median-based ALT is around 0.98 m which is projected to increase between 1.2 and 2.1 m by the end of the century depending on the emission scenario. This range further increases to 1.0–3.5 m depending on scenario if we consider the 5th and 95th based ALT. Under the low emission scenario SSP1-26, the ALT increases gradually until 2050 and then remains almost constant until 2100, reaching a value of 1.22 m (or a maximum of 1.5 m based on the 95th percentile value). As per our estimates, the SSP2-45 scenario would result in deepening of ALT to a maximum depth of about 1.5 m (or a maximum of 2.1 m as per 95th percentile) while SSP3-70 would lead to deepening of ALT to average depths of 1.8 m (max. 2.9 m) by the end of the twenty-first century. In the extreme scenario SSP5-85 (red line), median-based estimations lead to deepening of ALT up to 2.1 m (maximum of 3.5 m) by the year 2100.

Figure 5 shows a comparison of ALT estimated from four CMIP5 models under RCP-8.5 scenarios, and ensemble means of these models with ensemble mean ALT of CMIP6 models based on median ALT_{sensitivity} under SSP5-85. The

pink shaded area represents the range (5 to 95 percentiles) of hemispheric mean ALT of CMIP6 models and the solid lines show the median value of ALT_{sensitivity} (Sect. 2). Although the sample size of CMIP5 models (4) and CMIP6 models (34) is quite different, the ensemble mean ALT shows a similar decreasing trend with slight difference after 2050 under RCP-8.5 / SSP5-85 scenarios till end of the century. This again supports our hypothesis that ALT estimates from CMIP5 and CMIP6 show similar trends in the future.

Figure 6 shows spatial distribution of ensemble mean ALT of 34 models, for the year 2100 based on 5th percentile values of the ALT_{sensitivity} for the four future scenarios (SSP1-26, SSP2-45, SSP3-70 and SSP5-85). The deepening of ALT remains consistent across all scenarios, indicating significant permafrost thawing in low latitudes and relatively less thawing towards the poles. Nunavut, Canada's northernmost territory, and northern regions of Russia stay mainly frozen by the end of the century under SSP1-26 and SSP-245. However, SSP3-70 and SSP5-85 scenarios show thawing of permafrost in the northwestern part of Russia even when estimates are based on lower percentiles of ALT sensitivity. These 5th percentile ALT estimates represent the minimum thawing predicted by a set of CMIP6 models by the year 2100.

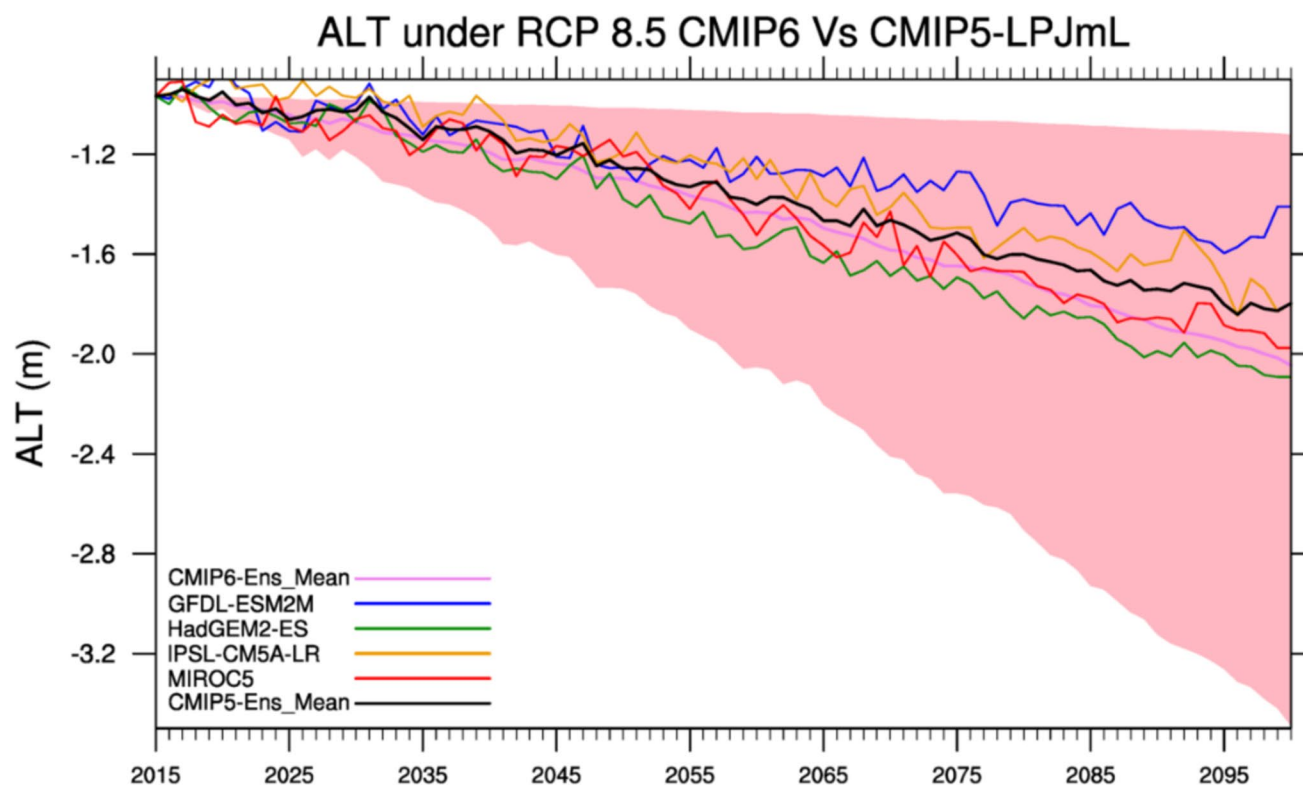
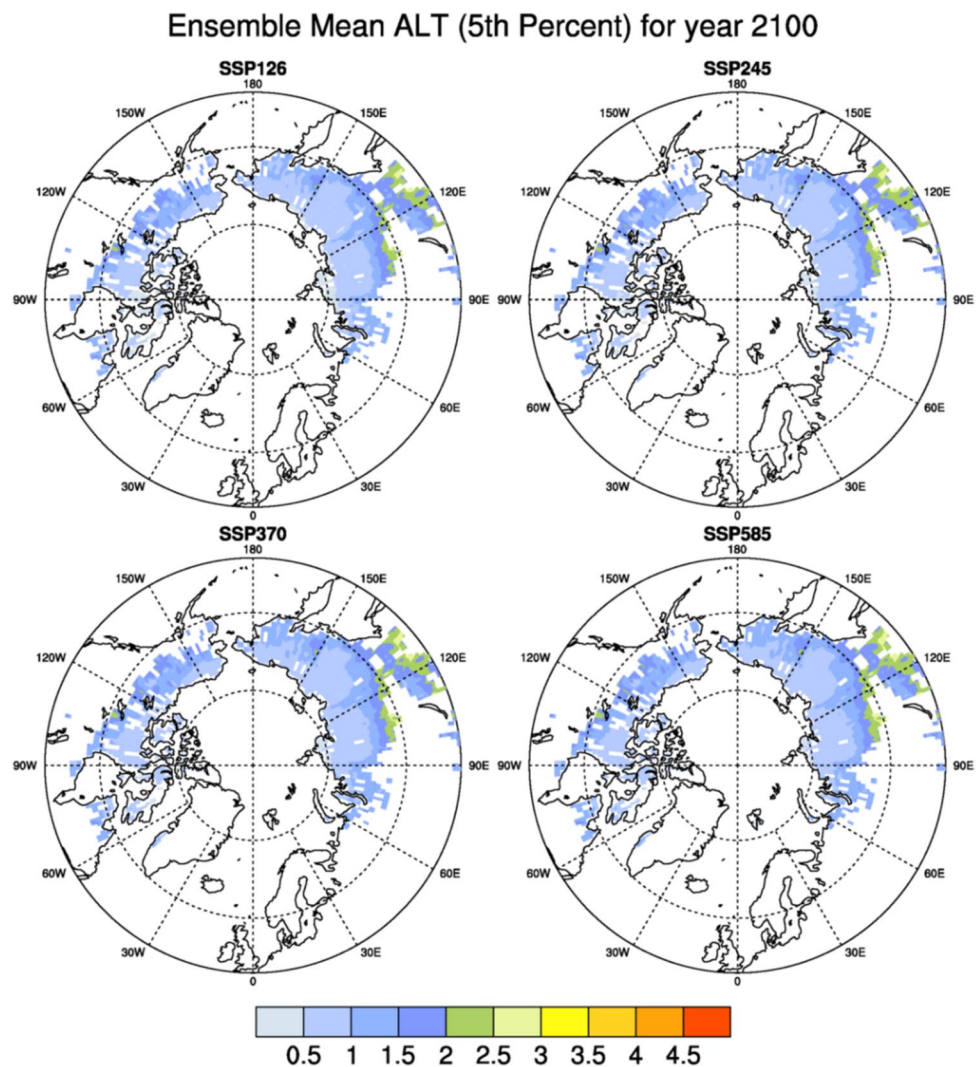


Fig. 5 Mean ALT of the permafrost area for the years 2015–2100. The shaded area represents the spread of CMIP6 models while solid lines represent the individual CMIP5 models and ensemble means (of 34 models) of median values

Fig. 6 Spatial distribution of ensemble mean ALT (m) based on 34 models under four scenarios at the end of the century, using the 5th percentile of $ALT_{sensitivity}$



The ensemble mean ALT of 34 models, based on 50th percentile (median) of $ALT_{sensitivity}$, are presented in Fig. 7 for the four future scenarios. Compared to the previous estimations based on 5th percentile of $ALT_{sensitivity}$, the thawing is more widespread and reaches northernmost regions of Canada and Russia even in low emission scenario SSP1-26. The warming pattern is similarly strong in the low latitudes and becomes weaker towards the pole. Under the highest emission scenario SSP5-85, the ALT reaches depths of 3.0 to 3.5 m in central Russia.

Figure 8 shows the ensemble mean ALT of 34 models for the four scenarios based on estimates on 95th value of $ALT_{sensitivity}$. The permafrost thawing presented here is the maximum thawing expected from a set of global climate models participating in CMIP6. The gradual increase in warming from low emission scenario SSP1-26 to high emission scenario SSP5-85 can be seen from similar trends in increase in global temperature scenarios for permafrost

region in Fig. 1. The latitudinal trend of the dependence of ALT towards the pole becomes stronger when higher values of $ALT_{sensitivity}$ are used for estimations.

The evolution of ALT deepening on a yearly basis is presented in Fig. 9 for each participating global climate model for the period 2015–2100. The x-axis represents the years, the y-axis displays different models, and missing data is highlighted by white lines. While this figure clearly shows the magnitude of thawing presented by each model and spread among the models, the year-to-year variations in ALT do not provide a clear understanding of changes in ALT. Decadal maximum ALT is a better measure to quantify the carbon present in thawing permafrost.

Figure 10 shows the decadal evolution of ALT changes in the twenty-first century. Again, the ALT are based on median values of $ALT_{sensitivity}$. These results add to Fig. 4 where only absolute values of ALT are shown. Here we show the anomalies in ALT as compared to ALT_b (base

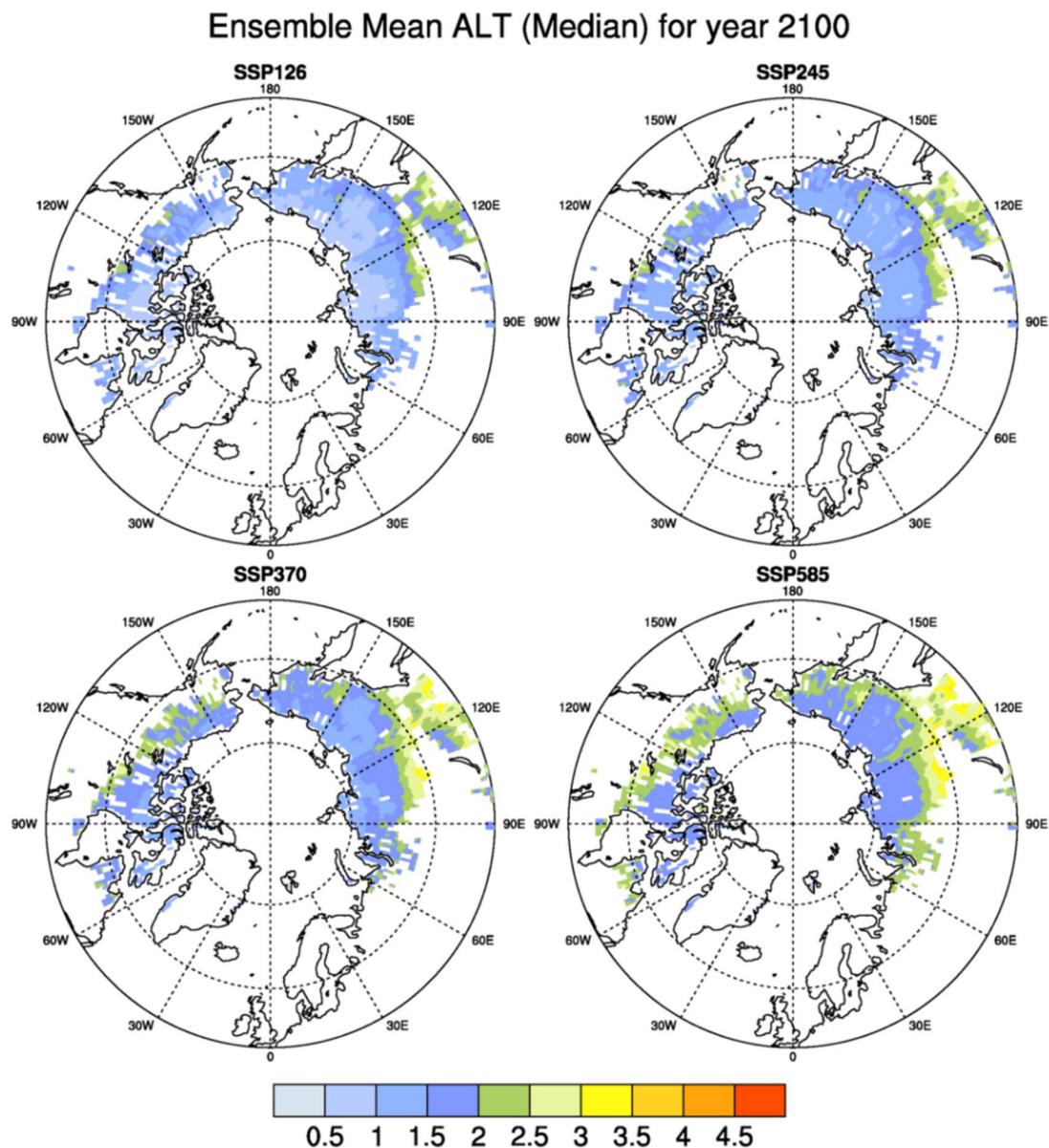
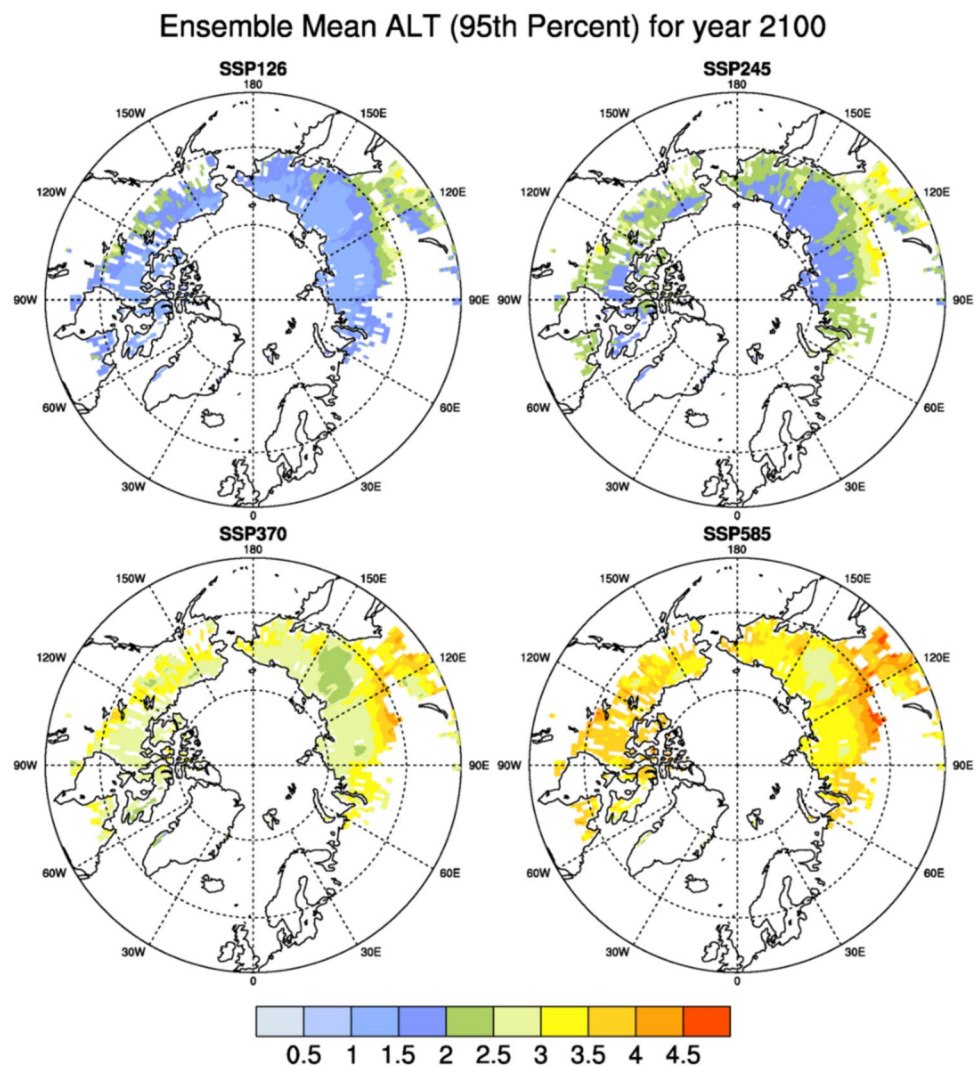


Fig. 7 Spatial distribution of ensemble mean ALT (m) based on 34 models under four scenarios at the end of the century, using the 50th percentile (median) of $ALT_{\text{sensitivity}}$

period ALT for the period 2011–2015). The box plots are based on median, 25th and 75th percentiles of ALT anomalies predicted by the models while the whiskers represent the minimum and maximum of the ensemble means, so that they present the full spread among the climate models. The gradual increase in ALT is seen under all scenarios except SSP1-26, where after mid-century the thawing seems to cease owing to stabilising temperatures. Contrary to this, the other three scenarios predict steady increases of thaw depth till the end of the century. The ensemble-mean ALT anomalies predicted by SSP1-26, SSP2-45, SSP3-70 and SSP5-85 are 0.3, 0.5, 0.8 and 1.0 m respectively by the end of the twenty-first century.

The estimates of vulnerable carbon ready for decomposition in the thawed permafrost are based on changes in maximum decadal ALT of each model. Using the 3D profile of carbon stocks (described in Section 3d), the amount of vulnerable carbon is estimated for every layer of thawed permafrost in each model on a decadal scale. Finally, the total carbon present in thawed permafrost is aggregated over the northern circumpolar region and the results are shown in Fig. 11. It shows that accumulated vulnerable carbon in thawing permafrost by the 2100 is estimated to be 40–230 GtC, 95–265 GtC, 101–400 GtC and 140–460 GtC under SSP1-26, SSP2-45, SSP3-70 and SSP5-85 respectively. The median estimates of total decomposable

Fig. 8 Spatial distribution of ensemble mean ALT (m) based on 34 models under four scenarios at the end of the century, using the 95th percentile of ALT_{sensitivity}



carbon by the end of century under the four scenarios are 115, 180, 260 and 300 GtC.

5 Discussion

The coupled global climate models used in CMIP6, like their CMIP5 predecessors, continue to face significant challenges in representing permafrost carbon-climate feedbacks. A key limitation is the inadequate simulation of subsurface parameters, particularly soil temperature profiles, and the absence of water phase-change processes, which are crucial for accurately simulating ALT. While some models with deeper soil layers, such as those discussed by Steinert et al. (2021), have improved thermodynamic representations, many still fail to include

critical processes like the latent heat dynamics associated with freezing and thawing. This results in overestimations of ALT, a problem highlighted by Peng et al. (2023), who noted that future ALT increases are inevitable but may be exaggerated by Earth System Models. Our analysis demonstrates that ALT sensitivity to MAAT across CMIP6 models reveals a range of ensemble-mean sensitivities at the 5th, 50th, and 95th percentiles of 0.02, 0.11, and 0.28 m/°C, respectively. These values align with CMIP5 estimates from Burke et al. (2013), suggesting that the underlying physics in the LSMs has seen limited evolution.

The corrected ALT estimates in our study are lower than the uncorrected CMIP6 projections and align more closely with observed ALT values, highlighting the importance of adjustments in future projections. This improvement stems

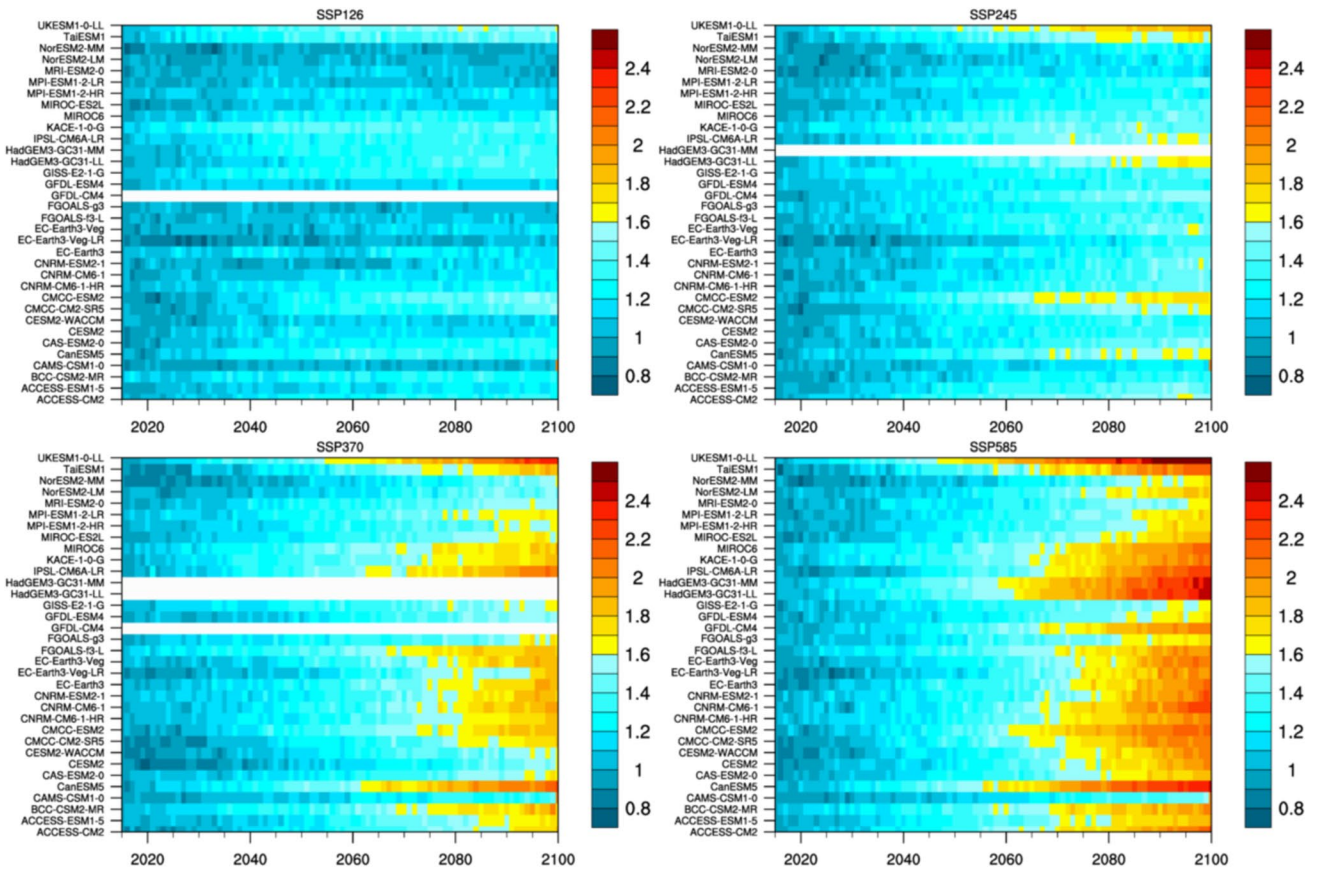
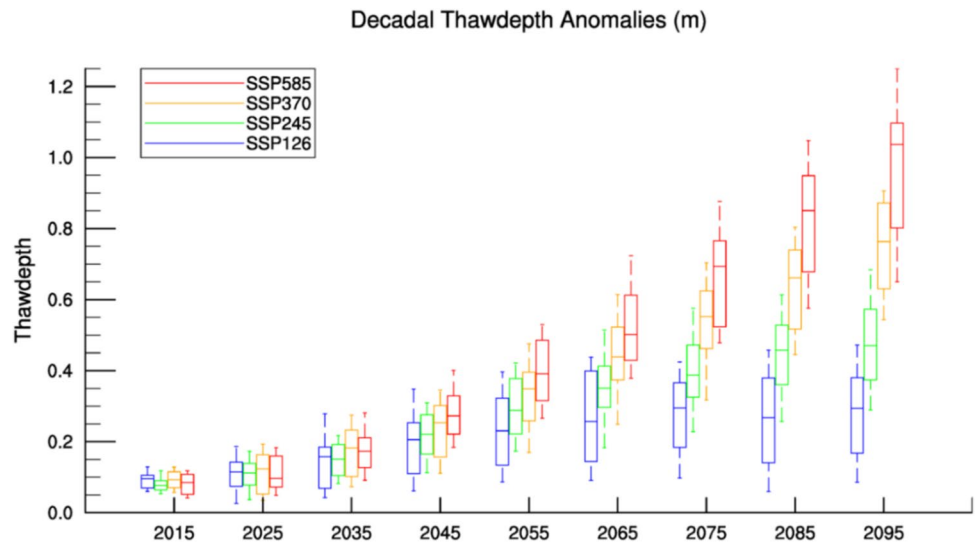


Fig. 9 Temporal development of ALT thickness (m) for 34 model, under four scenarios based on median value of ALT_{sensitivity}

Fig. 10 Decadal Thaw depth (m) anomalies from ALTb



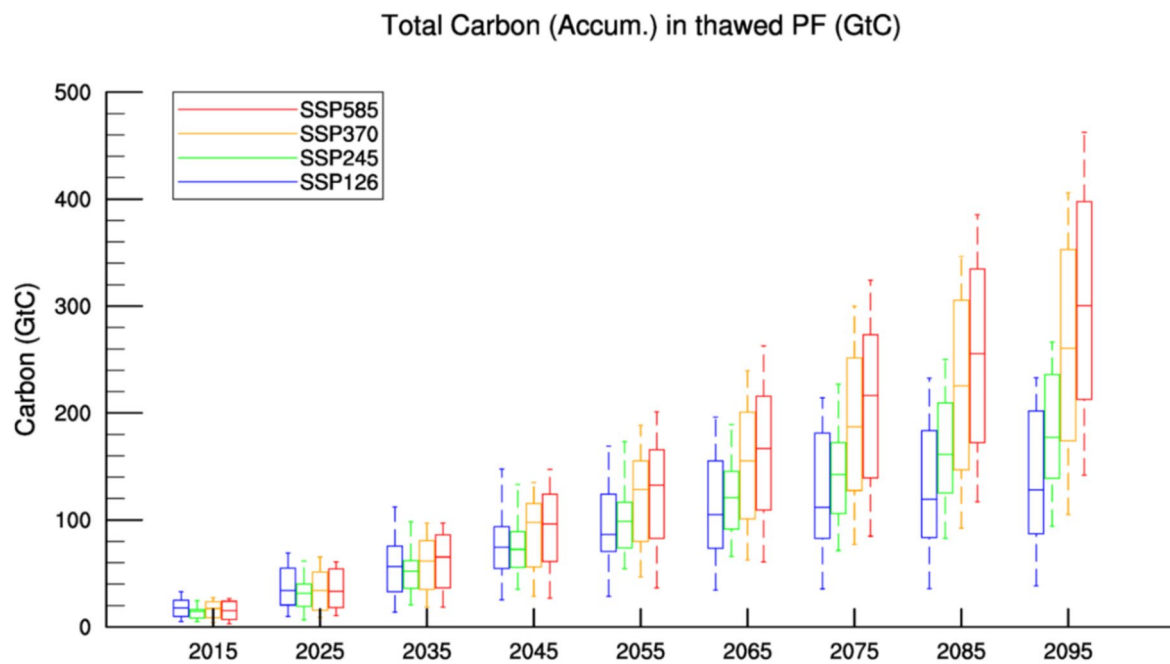


Fig. 11 Accumulated Carbon stocks estimated in thawed permafrost based on decadal maximum ALT

from bias-corrected estimates being derived from an indirect method based on MAAT and utilizing the median value of ALT sensitivity from a set of CMIP6 models. As a result, these estimates are not affected by the limitations of simplified LSMs in CMIP6. The median-based ALT approach mitigates the influence of outliers, ensuring more accurate projections, as validated against ESA Permafrost CCI records. Furthermore, the use of median-based ALT sensitivity is also supported by the output of the global vegetation model LPJmL.

Our findings indicate that the median-based ALT for the present day is approximately 0.98 m, projected to increase to a range of 1.2–2.1 m by 2100, depending on the emission scenario. Even under the low-emission scenario (SSP1-2.6), significant thawing is expected in low-latitude permafrost regions, with more widespread thawing observed in central Russia under the extreme emission scenario (SSP5-8.5). A clear latitudinal gradient emerges, with the most pronounced thawing occurring under the extreme SSP5-8.5 scenario and the 95th percentile-based ALT, particularly in Nunavut, Canada's northernmost territory, and the northern regions of Russia, where ALT may reach depths of up to 4 m. This extensive thawing in high-latitude regions poses substantial risks of releasing large quantities of greenhouse gases (CO_2 and CH_4), further accelerating global warming. These processes are likely to trigger significant changes in northern

ecosystems, including infrastructure damage, land subsidence, and widespread shifts in flora and fauna.

Historical studies have shown similar vulnerabilities of permafrost to warming climates. Nitzbon et al. (2024) highlighted that although the overall response of permafrost to climate change is gradual, differing local climates, environmental conditions, and regional isolation will result in local tipping points being reached at different times. Chadburn et al. (2015), using the JULES model, projected that near-surface permafrost area may halve by the end of the twenty-first century. Similarly, Chadburn et al. (2017) emphasized that even moderate levels of global warming could lead to substantial permafrost degradation. Limiting global temperature increases to 1.5 °C instead of 2 °C could prevent approximately 2 million square kilometers of permafrost from thawing. In extreme warming scenarios (5 °C or 6 °C above pre-industrial levels), nearly all permafrost is expected to thaw, leaving only 0.3–3.1 million square kilometers at 5 °C and 0.0–1.5 million square kilometers at 6 °C.

This study provides decadal-scale estimates of ALT changes and vulnerable carbon stocks, addressing a key gap in previous research. The decadal maximum values were used to quantify the carbon available for decomposition in thawing permafrost, and 3D carbon profiles were employed to estimate vulnerable carbon in each layer. Our study is the first to offer a comprehensive decadal analysis

of vulnerable carbon projections across different scenarios using a multi-model ensemble. These estimates reveal that, by 2100, the amount of decomposable carbon in thawed permafrost will be 40–230 GtC under the low-emission scenarios SSP1-2.6, 95–265 GtC under SSP2-4.5, 101–400 GtC under SSP3-7.0, and substantially higher values of 140–460 GtC under the high-emission scenario SSP5-8.5. These projections highlight the potential carbon release from thawed permafrost under varying climate scenarios.

Although we have quantified the amount of vulnerable carbon in thawed permafrost, it is crucial to acknowledge that our study does not account for the rate of carbon release following thawing. Uncertainties persist regarding the long-term behavior of thawed permafrost carbon stocks, influenced by factors such as the distribution between fast- and slow-decomposing carbon pools. Previous studies (e.g., Zimov et al. 2006) suggest that freshly thawed permafrost could lose up to 40% of its carbon within the first decade, significantly contributing to the permafrost carbon feedback. Moreover, abrupt thawing events may further accelerate carbon release and should be considered for a more comprehensive understanding of the permafrost carbon cycle (Turetsky et al. 2020). Future research should incorporate these processes, along with more advanced carbon release models like the PInc-Pan-Ther approach (Koven et al. 2015), to improve the accuracy of predictions.

6 Conclusions

This study highlights the ongoing degradation of permafrost in the Northern Hemisphere and the subsequent potential release of large amounts of carbon stored as soil organic carbon (SOC) in the form of CO₂ and methane. As global temperatures continue to rise, thawing permafrost is expected

to deepen significantly, contributing to positive feedback loops that further exacerbate climate change. Using CMIP6 models, we demonstrate that the projected changes in active layer thickness (ALT) are substantial. Comparisons of present-day ALT estimates with observed values underline the complexities in accurately simulating permafrost dynamics. However, our bias-corrected estimates of ALT, derived from these models, provide a more accurate representation of permafrost thaw, revealing potential discrepancies in the uncorrected estimation of vulnerable carbon stocks.

The predicted ALT deepening of 1.2–2.1 m across northern high latitudes by 2100 under different climate scenarios points to significant permafrost thawing, with profound thawing observed in low latitudes and extending toward the poles. With these projections and utilizing 3D profiles of carbon stocks, our decadal-scale estimates of vulnerable carbon in thawed permafrost provide robust projections, ranging from 115 GtC under SSP1-2.6 to 300 GtC under SSP5-8.5. These represent the amounts of carbon that could become susceptible to decomposition, posing a critical risk to global climate stability.

These findings highlight the need for further refinement in permafrost processes within climate models to better predict the role of permafrost in future climate change. Improving climate models to capture subsurface processes such as soil temperature profiles and water phase changes is essential for enhancing predictions of permafrost thaw and its contribution to the global carbon budget, which is crucial for mitigating the broader impacts of climate change.

Appendix

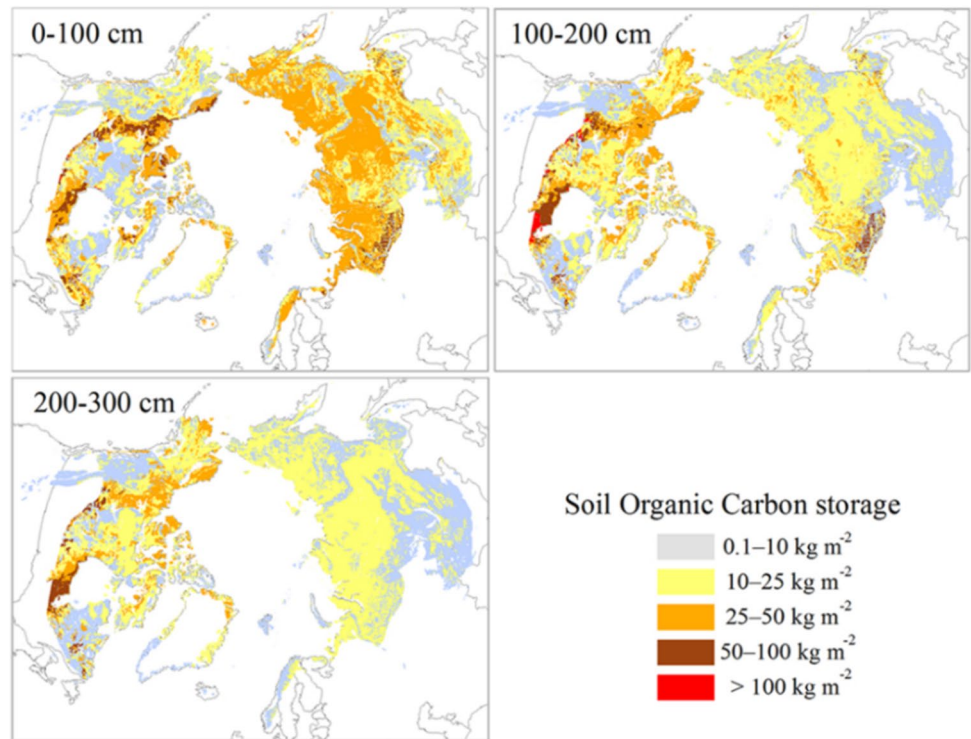
See below the Appendix Table 5; Figs. 12, 13, 14, 15, 16, 17

Table 5 The 5th and 95th percentile of ALT sensitivity in m/K for each model using all four scenarios

ALT Sensitivity	5th Percentile					95th Percentile				
	Hist	SSP126	SSP245	SSP370	SSP585	Hist	SSP126	SSP245	SSP370	SSP585
ACCESS-CM2	0.015	0.013	0.013	0.014	0.023	0.247	0.296	0.297	0.233	0.193
ACCESS-ESM1-5	0.013	0.014	0.015	0.016	0.016	0.365	0.337	0.300	0.280	0.278
BCC-CSM2-MR	0.017	0.014	0.014	0.014	0.016	0.243	0.198	0.218	0.218	0.216
CAMS-CSM1 -0	0.013	0.013	0.013	0.013	0.013	0.188	0.174	0.166	0.164	0.174
CanESM5	0.014	0.014	0.016	0.018	0.019	0.343	0.416	0.450	0.311	0.313
CAS-ESM2-0	0.012	0.017	0.016	0.015	0.014	0.132	0.281	0.222	0.200	0.177
CESM2	0.043	0.051	0.059	0.051	0.033	0.304	0.337	0.407	0.358	0.313
CESM2-WACCM	0.049	0.044	0.057	0.046	0.028	0.311	0.332	0.404	0.345	0.295
CMCC-CM2-SR5	0.021	0.013	0.016	0.014	0.013	0.277	0.312	0.326	0.335	0.291
CMCC-ESM2	0.031	0.016	0.015	0.012	0.015	0.277	0.313	0.299	0.288	0.271
CNRM-CM6-1	0.042	0.056	0.061	0.058	0.045	0.174	0.222	0.254	0.242	0.246
CNRM-CM6-1-H R	0.036	0.044	0.052	0.046	0.030	0.164	0.193	0.220	0.207	0.200
CNRM-ESM2-1	0.041	0.051	0.058	0.052	0.032	0.168	0.152	0.205	0.206	0.212
EC-Earth3	0.017	0.015	0.013	0.012	0.012	0.170	0.148	0.148	0.159	0.143
EC-Earth3-Veg-LR	0.015	0.014	0.012	0.012	0.012	0.163	0.176	0.177	0.156	0.140
EC-Earth3-Veg	0.000	0.014	0.013	0.012	0.012	0.000	0.141	0.145	0.144	0.145
FGOALS-f3-L	0.020	0.021	0.030	0.029	0.026	0.207	0.173	0.273	0.229	0.225
FGOALS-g3	0.012	0.016	0.024	0.023	0.023	0.115	0.157	0.222	0.241	0.234
GFDL-CM4	0.019	0.000	0.027	0.000	0.032	0.279	0.000	0.340	0.000	0.226
GFDL-ESM4	0.014	0.015	0.018	0.026	0.026	0.262	0.302	0.375	0.375	0.325
GISS-E2-1-G	0.022	0.016	0.024	0.023	0.021	0.257	0.150	0.302	0.308	0.294
HadGEM3-GC31-LL	0.015	0.012	0.013	0.000	0.015	0.200	0.213	0.208	0.000	0.187
HadGEM3-GC31-MM	0.014	0.012	0.000	0.000	0.013	0.192	0.216	0.000	0.000	0.187
IPSL-CM6A-LR	0.020	0.016	0.021	0.019	0.021	0.244	0.355	0.426	0.407	0.384
KACE-1-0-G	0.013	0.018	0.017	0.017	0.015	0.371	0.403	0.393	0.413	0.421
MIROC6	0.014	0.014	0.017	0.025	0.024	0.210	0.306	0.306	0.266	0.268
MIROC-ES2L	0.013	0.015	0.019	0.021	0.024	0.211	0.317	0.338	0.314	0.329
MPI-ESM1 -2-HR	0.043	0.036	0.031	0.036	0.034	0.218	0.230	0.276	0.259	0.267
MPI-ESM1-2-LR	0.047	0.033	0.042	0.042	0.035	0.197	0.221	0.252	0.249	0.248
MRI-ESM2-0	0.021	0.018	0.024	0.033	0.028	0.158	0.209	0.256	0.246	0.229
NorESM2-LM	0.038	0.032	0.050	0.042	0.019	0.285	0.246	0.299	0.283	0.230
NorESM2-MM	0.039	0.035	0.049	0.044	0.041	0.296	0.272	0.338	0.331	0.297
TaiESM1	0.024	0.044	0.044	0.029	0.023	0.166	0.275	0.271	0.303	0.314
UKESM1-0-LL	0.016	0.012	0.012	0.011	0.011	0.190	0.146	0.124	0.130	0.151

The historical period here refers to 1950–2014, and the scenarios data is used for the period 2015–2100

Fig. 12 Estimated soil organic carbon storage (kg C m^2) in the 0–1 m, 1–2 m and 2–3 m depth ranges of the northern circumpolar permafrost region. Source: Hugelius et al. (2013)



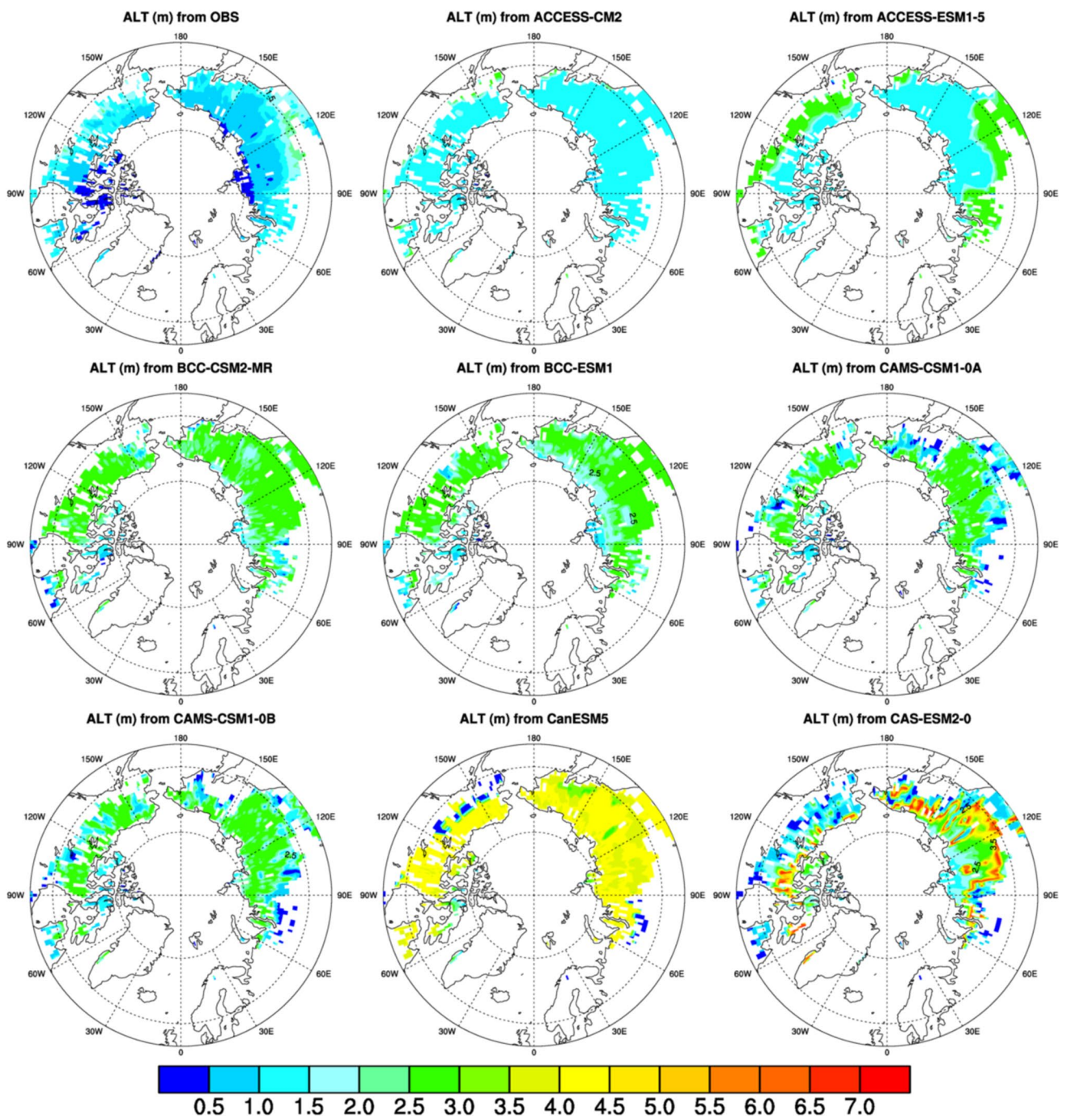


Fig. 13 Comparison of ALT calculated from CMIP6 models (using soil temperature) with Observations (part1)

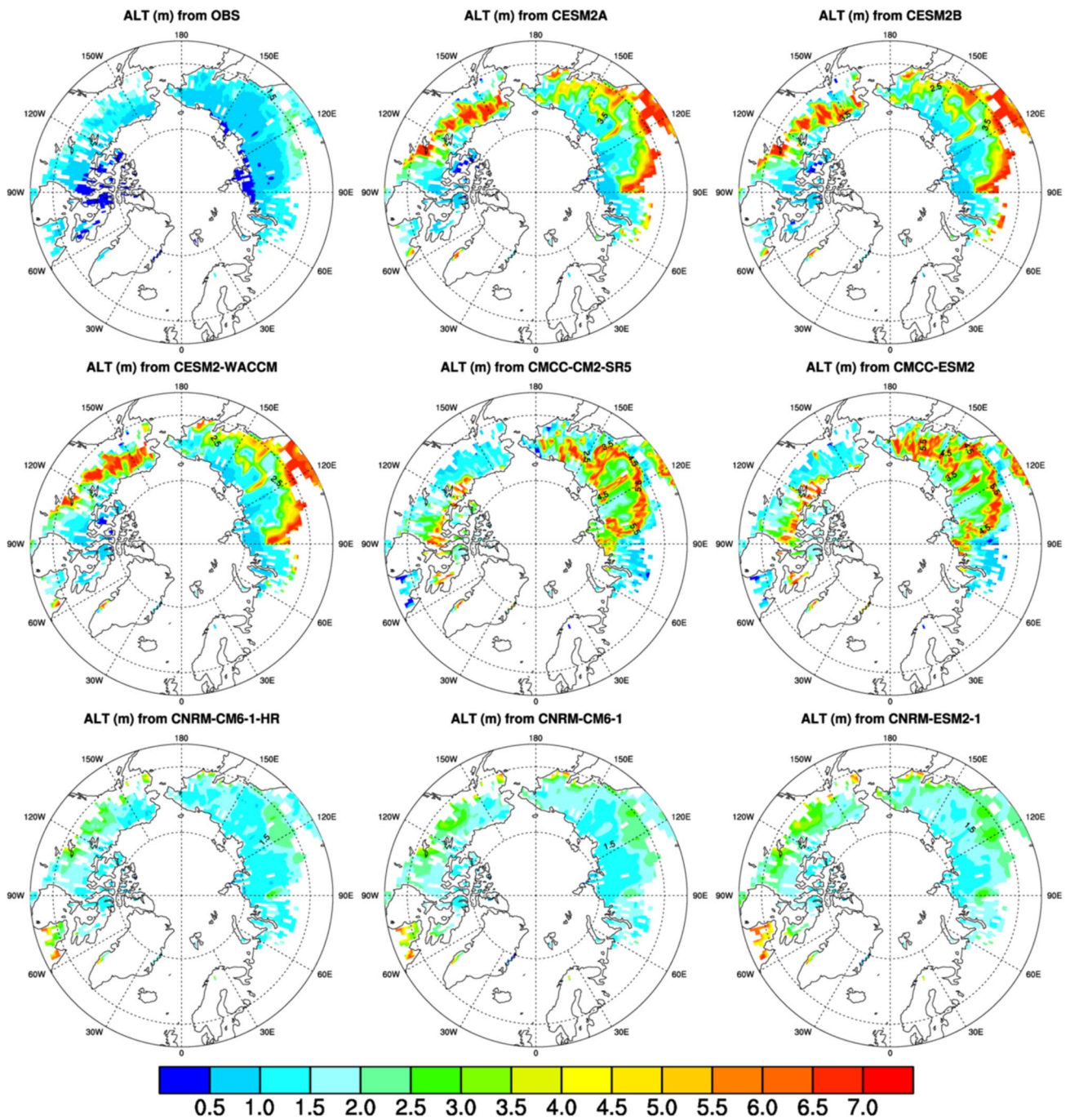


Fig. 14 Comparison of ALT calculated from CMIP6 models (using soil temperature) with Observations (part2)

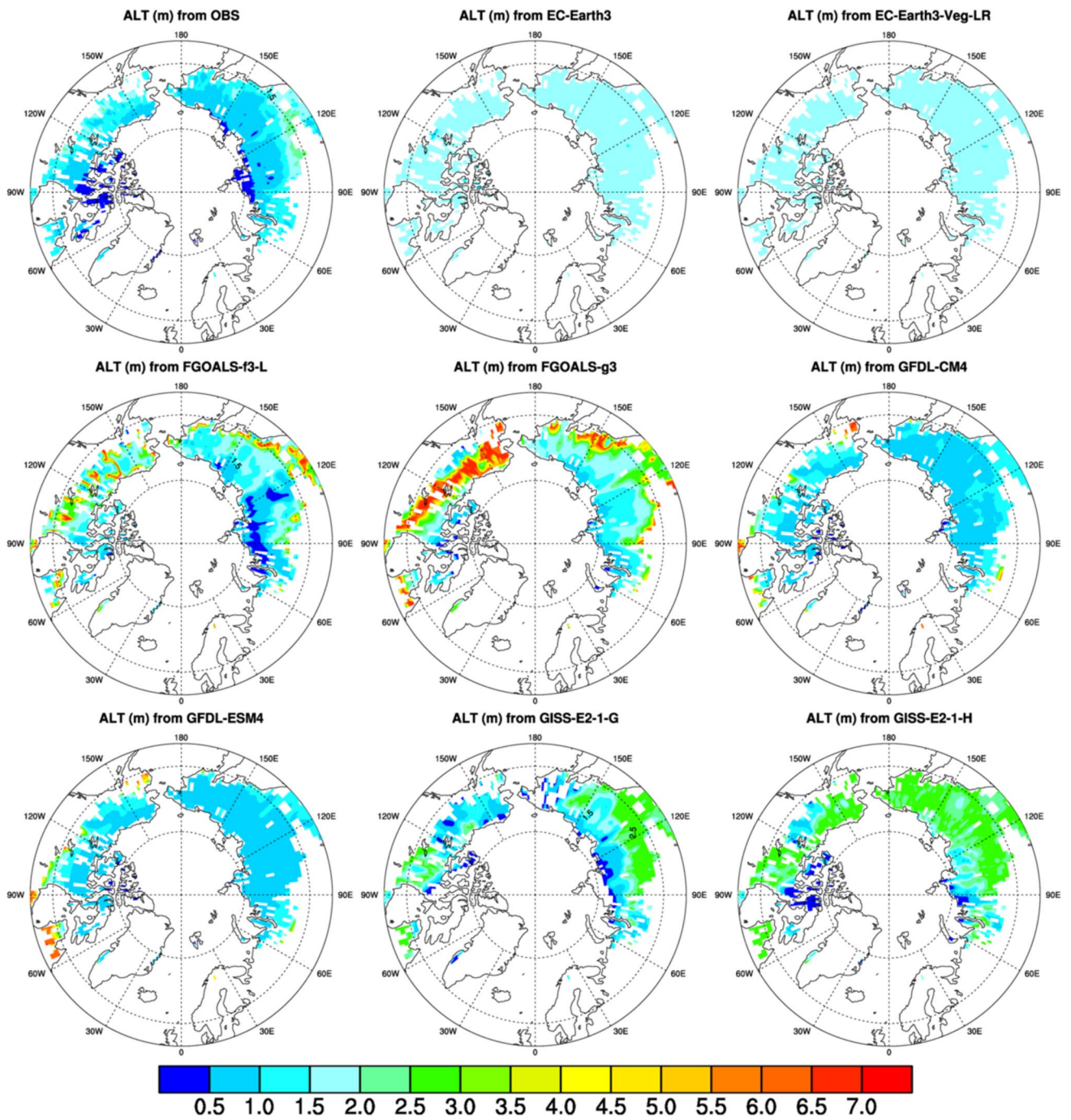


Fig. 15 Comparison of ALT calculated from CMIP6 models (using soil temperature) with Observations (part3)

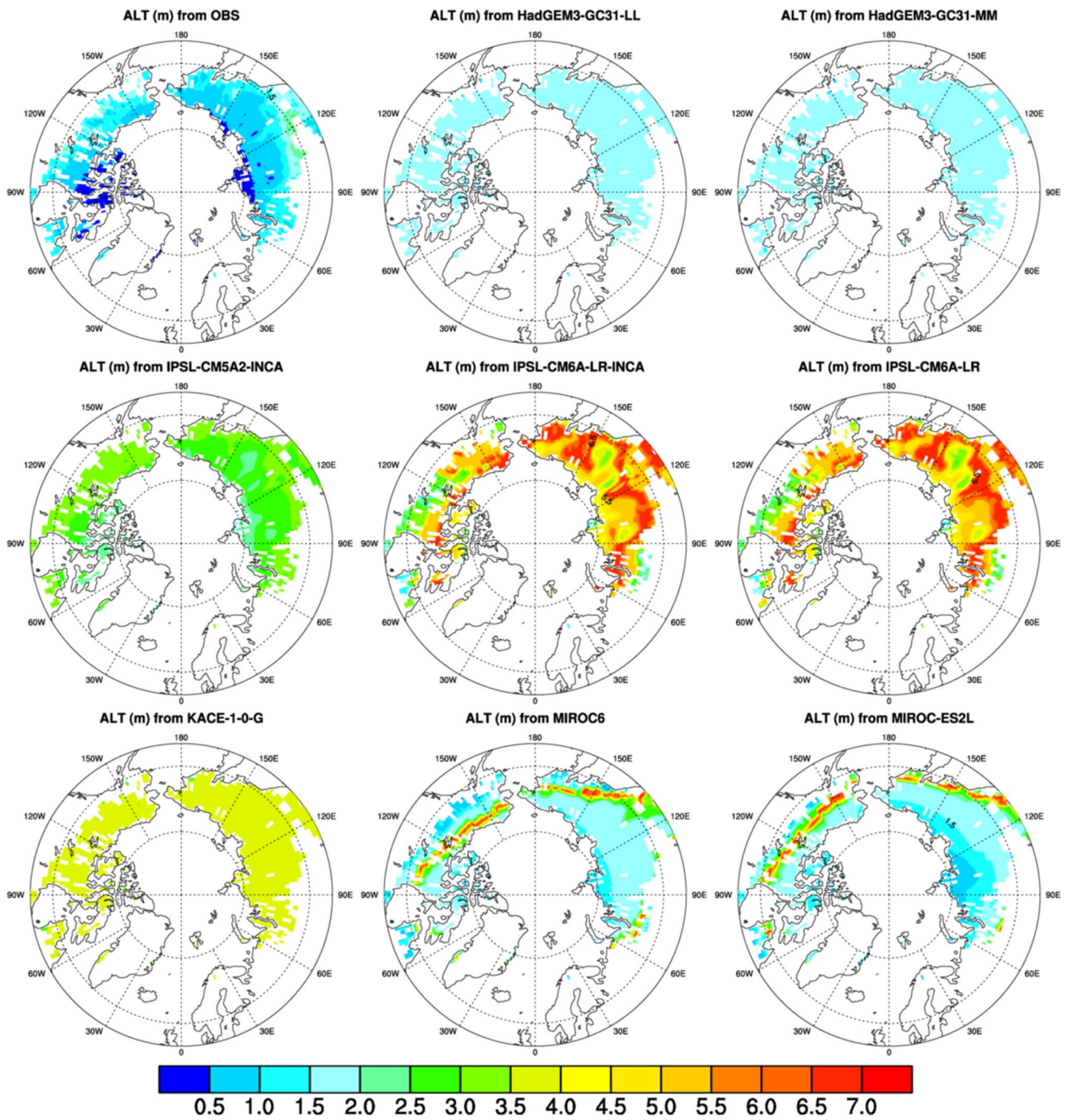


Fig. 16 Comparison of ALT calculated from CMIP6 models (using soil temperature) with Observations (part4)

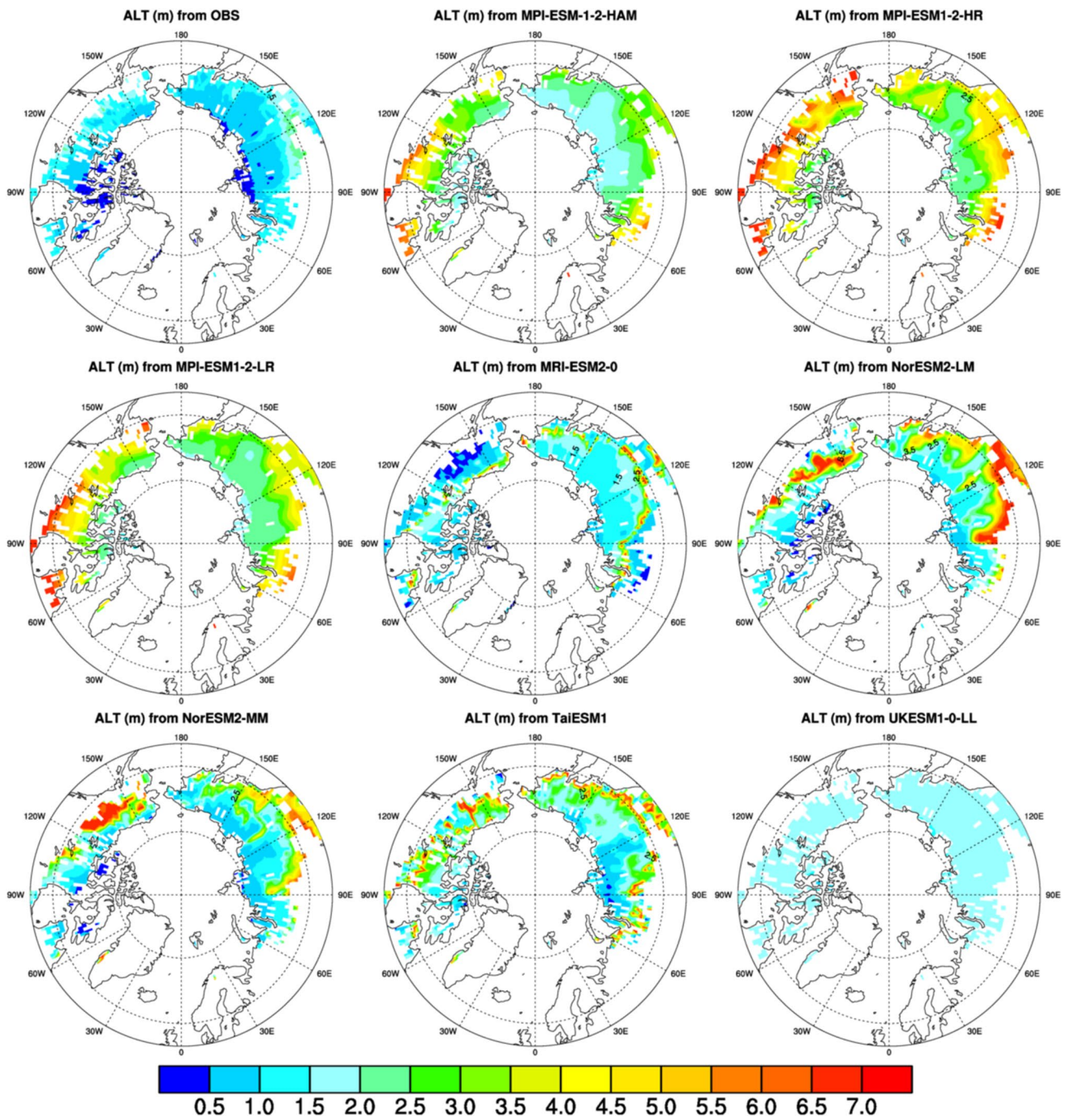


Fig. 17 Comparison of ALT calculated from CMIP6 models (using soil temperature) with Observations (part5)

Acknowledgements We would like to extend our sincere gratitude to the two anonymous reviewers for their insightful comments and thorough recommendations, which have greatly improved the quality and clarity of this work. Their incisive criticism and in-depth assessments greatly helped us improve the overall integrity of our work and refine our analysis. We profoundly appreciate them for their contributions to this research.

Funding Open access funding provided by University of Natural Resources and Life Sciences Vienna (BOKU). This work is part of the Earth Commission which is hosted by Future Earth and is the science component of the Global Commons Alliance. The Global Commons Alliance is a sponsored project of Rockefeller Philanthropy Advisors, with support from Oak Foundation, MAVA, Porticus, Gordon and Betty Moore Foundation, Tiina and Antti Herlin Foundation, William and Flora Hewlett Foundation, and the Global Environment Facility. The Earth Commission is also supported by the Global Challenges Foundation, Frontiers Research Foundation and FORMAS – a Swedish Research Council for Sustainable Development (2022–02686).

Data Availability The datasets generated during the current study are available from the corresponding author on reasonable request.

Declarations

Conflict of Interest The authors declare that they have no conflicts of interest regarding the publication of this manuscript in Earth Systems and Environment. Any financial or personal relationships with other people or organizations that could inappropriately influence the work have been disclosed.

Ethics Statement The research and manuscript follow strict ethical guidelines, according to the ethics statement. The rights of human subjects and animal welfare were upheld. Confidentiality was upheld and informed consent was acquired. The information is true, and any potential conflicts of interest have been declared. Integrity, openness, and reproducibility were given top priority.

Open Access This article is licensed under a Creative Commons Attribution 4.0 International License, which permits use, sharing, adaptation, distribution and reproduction in any medium or format, as long as you give appropriate credit to the original author(s) and the source, provide a link to the Creative Commons licence, and indicate if changes were made. The images or other third party material in this article are included in the article's Creative Commons licence, unless indicated otherwise in a credit line to the material. If material is not included in the article's Creative Commons licence and your intended use is not permitted by statutory regulation or exceeds the permitted use, you will need to obtain permission directly from the copyright holder. To view a copy of this licence, visit <http://creativecommons.org/licenses/by/4.0/>.


References

- Armstrong McKay DI, Staal A, Abrams JF, Winkelmann R, Sak-schewski B, Loriani S et al (2022) Exceeding 1.5 °C global warming could trigger multiple climate tipping points. *Science* 377:eabn7950. <https://doi.org/10.1126/science.abn7950>
- Boucher O, Servonnat J, Albright AL, Aumont O, Balkanski Y, Bastrikov V et al (2020) Presentation and evaluation of the IPSL-CM6A-LR climate model. *J Adv Model Earth Syst.* <https://doi.org/10.1029/2019MS002010>
- Braghiere RK, Fisher JB, Miner KR, Miller CE, Worden JR, Schimel DS, Frankenberg C (2023) Tipping point in North American Arctic-Boreal carbon sink persists in new generation Earth system models despite reduced uncertainty. *Environ Res Lett* 18(2):025008. <https://doi.org/10.1088/1748-9326/acb226>
- Burke EJ, Hartley IP, Jones CD (2012) Uncertainties in the global temperature change caused by carbon release from permafrost thawing. *Cryosphere* 6:1063–1076. <https://doi.org/10.5194/tc-6-1063-2012>
- Burke EJ, Jones CD, Koven CD (2013) Estimating the permafrost-carbon climate response in the CMIP5 climate models using a simplified approach. *J Clim* 26:4897–4909. <https://doi.org/10.1175/JCLI-D-12-00550.1>
- Burke KD, Williams JW, Chandler MA, Haywood AM, Lunt DJ, Otto-Bliessner BL (2018) Pliocene and eocene provide best analogs for near-future climates. *Proc Natl Acad Sci* 115:13288–13293. <https://doi.org/10.1073/pnas.1809600115>
- Burke EJ, Zhang Y, Krinner G (2020) Evaluating permafrost physics in the Coupled Model Intercomparison Project 6 (CMIP6) models and their sensitivity to climate change. *Cryosphere* 14:3155–3174. <https://doi.org/10.5194/tc-14-3155-2020>
- Chadburn SE, Burke EJ, Essery RLH, Boike J, Langer M, Heikenfeld M, Cox PM, Friedlingstein P (2015) Impact of model developments on present and future simulations of permafrost in a global land-surface model. *Cryosphere* 9(4):1505–1521. <https://doi.org/10.5194/tc-9-1505-2015>
- Chadburn S, Burke E, Cox P et al (2017) An observation-based constraint on permafrost loss as a function of global warming. *Nature Clim Change* 7:340–344. <https://doi.org/10.1038/nclimate3262>
- Cosby BJ, Hornberger GM, Clapp RB, Ginn TR (1984) A statistical exploration of the relationships of soil moisture characteristics to the physical properties of soils. *Water Resour Res* 20:682–690. <https://doi.org/10.1029/WR020i0006p00682>
- Dunne JP, John JG, Adcroft AJ, Griffies SM, Hallberg RW, Shevliakova E et al (2012) GFDL's ESM2 global coupled climate-carbon earth system models. Part I: physical formulation and baseline simulation characteristics. *J Clim* 25:6646–6665. <https://doi.org/10.1175/JCLI-D-11-00560.1>
- Ekici A, Beer C, Hagemann S, Boike J, Langer M, Hauck C (2014) Simulating high-latitude permafrost regions by the JSBACH terrestrial ecosystem model. *Geosci Model Dev* 7(2):631–647. <https://doi.org/10.5194/gmd-7-631-2014>
- Eyring V, Bony S, Meehl GA, Senior CA, Stevens B, Stouffer RJ, Taylor KE (2016) Overview of the Coupled Model Intercomparison Project Phase 6 (CMIP6) experimental design and organization. *Geosci Model Dev* 9:1937–1958. <https://doi.org/10.5194/gmd-9-1937-2016>
- Fader M, Rost S, Müller C, Bondeau A, Gerten D (2010) Virtual water content of temperate cereals and maize: present and potential future patterns. *J Hydrol* 384:218–231. <https://doi.org/10.1016/j.jhydrol.2009.12.011>
- Frieler K, Lange S, Piontek F, Reyer CPO, Schewe J, Warszawski L et al (2017) Assessing the impacts of 1.5 °C global warming – simulation protocol of the Inter-Sectoral Impact Model Intercomparison Project (ISIMIP2b). *Geosci Model Dev* 10:4321–4345. <https://doi.org/10.5194/gmd-10-4321-2017>
- González-Rouco JF, Steinert NJ, García-Bustamante E, Hagemann S, de Vrese P, Jungclaus JH, Lorenz SJ, Melo-Aguilar C, García-Pereira F, Navarro J (2021) Increasing the depth of a Land Surface Model. Part I: Impacts on the soil thermal regime and energy storage. *J Hydrometeorol* 22(12):3211–3230. <https://doi.org/10.1175/JHM-D-21-0024.1>
- Guo D, Wang H (2016) CMIP5 permafrost degradation projection: a comparison among different regions. *J Geophys Res Atmos* 121(9):4499–4517. <https://doi.org/10.1002/2015JD024108>

- Harp DR, Atchley AL, Painter SL, Coon ET, Wilson CJ, Romanovsky VE, Rowland JC (2016) Effect of soil property uncertainties on permafrost thaw projections: a calibration-constrained analysis. *Cryosphere* 10:341–358. <https://doi.org/10.5194/tc-10-341-2016>
- Hermoso de Mendoza I, Beltrami H, Macdougall AH, Mareschal J-C (2020) Lower boundary conditions in land surface models-effects on the permafrost and the carbon pools: a case study with CLM4.5. *Geoscient Model Dev* 13(4):1663–1683. <https://doi.org/10.5194/gmd-13-1663-2020>
- Hjort J, Karjalainen O, Alto J, Westermann S, Romanovsky VE, Nelson FE et al (2018) Degrading permafrost puts Arctic infrastructure at risk by mid-century. *Nat Commun* 9:5147. <https://doi.org/10.1038/s41467-018-07557-4>
- Hugelius G, Bockheim JG, Camill P, Elberling B, Grosse G, Harden JW et al (2013) A new data set for estimating organic carbon storage to 3 m depth in soils of the northern circumpolar permafrost region. *Earth Syst Sci Data* 5:393–402. <https://doi.org/10.5194/essd-5-393-2013>
- Hugelius G, Strauss J, Zubrzycki S, Harden JW, Schuur EAG, Ping CL et al (2014) Estimated stocks of circumpolar permafrost carbon with quantified uncertainty ranges and identified data gaps. *Biogeosciences* 11:6573–6593. <https://doi.org/10.5194/bg-11-6573-2014>
- Koven CD, Riley WJ, Stern A (2013) Analysis of permafrost thermal dynamics and response to climate change in the CMIP5 earth system models. *J Clim* 26:1877–1900. <https://doi.org/10.1175/JCLI-D-12-00228.1>
- Koven CD, Schuur EAG, Schädel C, Bohn TJ, Burke EJ, Chen G et al (2015) A simplified, data-constrained approach to estimate the permafrost carbon–climate feedback. *Philos Trans Royal Soc Math Phys Eng Sci* 373:20140423. <https://doi.org/10.1098/rsta.2014.0423>
- Lange S (2018) Bias correction of surface downwelling longwave and shortwave radiation for the EWEMBI dataset. *Earth Syst Dynam* 9:627–645. <https://doi.org/10.5194/esd-9-627-2018>
- Lawrence DM, Slater AG (2005) A projection of severe near-surface permafrost degradation during the 21st century. *Geophys Res Lett* 32:L24401. <https://doi.org/10.1029/2005GL025080>
- Lenton TM, Held H, Kriegler E, Hall JW, Lucht W, Rahmstorf S, Schellnhuber HJ (2008) Tipping elements in the Earth's climate system. *Proc Natl Acad Sci* 105:1786–1793. <https://doi.org/10.1073/pnas.0705414105>
- Li C, Wei Y, Liu Y, Li L, Peng L, Chen J et al (2022) Active layer thickness in the Northern Hemisphere: changes from 2000 to 2018 and future simulations. *J Geophys Res Atmos*. <https://doi.org/10.1029/2022JD036785>
- Masson-Delmotte V, Zhai P, Pirani A, Connors SL, Péan C, Berger S et al (2021) Summary for policymakers. In: *Climate Change 2021: The Physical Science Basis. Contribution of Working Group I to the Sixth Assessment Report of the Intergovernmental Panel on Climate Change*. https://www.ipcc.ch/report/ar6/wg1/downloads/report/IPCC_AR6_WGI_SPM.pdf
- Meinshausen M, Smith SJ, Calvin K, Daniel JS, Kainuma MLT, Lamarque JF et al (2011) The RCP greenhouse gas concentrations and their extensions from 1765 to 2300. *Clim Change* 109:213–241. <https://doi.org/10.1007/s10584-011-0156-z>
- Miesner F, Overduin PP, Grosse G, Strauss J, Langer M, Westermann S et al (2023) Subsea permafrost organic carbon stocks are large and of dominantly low reactivity. *Sci Rep* 13(1):9425. <https://doi.org/10.1038/s41598-023-36471-z>
- Nachtergaele F, Van Velthuizen H, Verelst L, Batjes NH, Dijkshoorn K, Van Engelen VWP et al (2010) The harmonized world soil database. In *Proceedings of the 19th World Congress of Soil Science, Soil Solutions for a Changing World*, Brisbane, Australia
- Natali SM, Holdren JP, Rogers BM, Treharne R, Duffy PB, Pomerance R, MacDonald E (2021) Permafrost carbon feedbacks threaten global climate goals. *Proc Natl Acad Sci* 118:e202106114. <https://doi.org/10.1073/pnas.2100163118>
- Nitzbon J, Schneider von Deimling T, Aliyeva M et al (2024) No respite from permafrost-thaw impacts in the absence of a global tipping point. *Nat Clim Chang* 14:573–585. <https://doi.org/10.1038/s41558-024-02011-4>
- O'Neill BC, Tebaldi C, van Vuuren DP, Eyring V, Friedlingstein P, Hurtt G et al (2016) The scenario model intercomparison project (ScenarioMIP) for CMIP6. *Geosci Model Dev* 9:3461–3482. <https://doi.org/10.5194/gmd-9-3461-2016>
- Obu JW, Westermann S, Barboux C, Bartsch A, Delaloye R, Grosse G et al (2021) ESA permafrost climate change initiative (Permafrost_cci): permafrost active layer thickness for the Northern Hemisphere, v3.0. NERC EDS Centre for Environmental Data Analysis. <https://doi.org/10.5285/67a3f8c8dc914ef99f7f08eb0d997e23>
- Peng X, Zhang T, Frauenfeld OW, Mu C, Wang K, Wu X et al (2023) Active layer thickness and permafrost area projections for the 21st century. *Earth's Fut*. <https://doi.org/10.1029/2023EF003573>
- Rantanen M, Karpechko AY, Lipponen A, Nordling K, Hyvärinen O, Ruosteenoja K et al (2022) The Arctic has warmed nearly four times faster than the globe since 1979. *Commun Earth Environ* 3:168. <https://doi.org/10.1038/s43247-022-00498-3>
- Riahi K, Rao S, Krey V, Cho C, Chirkov V, Fischer G et al (2011) RCP 8.5—A scenario of comparatively high greenhouse gas emissions. *Clim Change* 109:33–57. <https://doi.org/10.1007/s10584-011-0149-y>
- Schaphoff S, von Bloh W, Rammig A, Thonicke K, Biemans H, Forkel M et al (2018a) LPJmL4 – a dynamic global vegetation model with managed land – Part 1: Model description. *Geosci Model Dev* 11:1343–1375. <https://doi.org/10.5194/gmd-11-1343-2018>
- Schaphoff S, Forkel M, Müller C, Knauer J, von Bloh W, Gerten D et al (2018b) LPJmL4 – a dynamic global vegetation model with managed land – Part 2: Model evaluation. *Geosci Model Dev* 11:1377–1403. <https://doi.org/10.5194/gmd-11-1377-2018>
- Schuur EAG, McGuire AD, Schädel C, Grosse G, Harden JW, Hayes DJ, Hugelius G, Koven CD, Kuhry P, Lawrence DM, Natali SM (2015) Climate change and the permafrost carbon feedback. *Nature* 520(7546):171–179. <https://doi.org/10.1038/nature14338>
- Schuur EAG, Abbott BW, Commans R, Ernakovich J, Euskirchen E, Hugelius G, Grosse G, Jones M, Koven C, Leshyk V, Lawrence D (2022) Permafrost and climate change: Carbon cycle feedbacks from the warming Arctic. *Annu Rev Environ Resour* 47:343–371. <https://doi.org/10.1146/annurev-environ-012220-011847>
- Steinert NJ, González-Rouco JF, Melo Aguilar C, García-Pereira C, García-Bustamante E, de Vrese P, Alexeev V, Jungclaus JH, Lorenz SJ, Hagemann S (2021) Agreement of analytical and simulation-based estimates of the required land depth in climate models. *Geophys Res Lett*. <https://doi.org/10.1029/2021GL094273>
- Steinert NJ, Debolskiy MV, Burke EJ, García-Pereira F, Lee H (2024) Evaluating permafrost definitions for global permafrost area estimates in CMIP6 climate models. *Environ Res Lett* 19(1):014033. <https://doi.org/10.1088/1748-9326/ad10d7>
- Strauss J, Schirrmeister L, Grosse G, Fortier D, Hugelius G, Knoblauch C, Romanovsky VE, Schädel C, Schneider von Deimling T, Schuur EAG, Shmelev D, Ulrich M, Veremeeva A (2017) Deep Yedoma permafrost: a synthesis of depositional characteristics and carbon vulnerability. *Earth Sci Rev* 172:75–86. <https://doi.org/10.1016/j.earscirev.2017.07.007>
- Taylor KE, Stouffer RJ, Meehl GA (2012) An Overview of CMIP5 and the experiment design. *Bull Am Meteor Soc* 93(4):485–498. <https://doi.org/10.1175/BAMS-D-11-00094.1>

- Turetsky MR, Abbott BW, Jones MC, Walter Anthony K, Olefeldt D, Schuur EAG, Koven C, McGuire AD, Grosse G, Kuhry P, Hugelius G, Lawrence DM, Gibson C, Sannel ABK (2019) Permafrost collapse is accelerating carbon release. *Nature* 569:32–34. <https://doi.org/10.1038/d41586-019-01313-4>
- Turetsky MR, Abbott BW, Jones MC, Anthony KW, Olefeldt D, Schuur EAG, Grosse G, Kuhry P, Hugelius G, Koven C, Lawrence DM (2020) Carbon release through abrupt permafrost thaw. *Nat Geosci* 13(2):138–143. <https://doi.org/10.1038/s41561-019-0526-0>
- Warszawski L, Frieler K, Huber V, Piontek F, Serdeczny O, Schewe J (2014) The Inter-Sectoral Impact Model Intercomparison Project (ISI-MIP): Project framework. *Proc Natl Acad Sci* 111:3228–3232. <https://doi.org/10.1073/pnas.1312330110>
- Zhang T, Frauenfeld OW, Serreze MC, Etringer A, Oelke C, McCreight J, Barry RG, Gilichinsky D, Yang D, Ye H, Ling F, Chudinova S (2005) Spatial and temporal variability in active layer thickness over the Russian Arctic drainage basin. *J Geophys Res Atmos*. <https://doi.org/10.1029/2004JD005642>
- Zhang T, Barry RG, Knowles K, Heginbottom JA, Brown J (2008) Statistics and characteristics of permafrost and ground-ice distribution in the Northern Hemisphere. *Polar Geogr* 31(1–2):47–68. <https://doi.org/10.1080/10889370802175895>
- Zimov SA, Schuur EAG, Chapin FS (2006) Permafrost and the global carbon budget. *Science* 312(5780):1612–1613. <https://doi.org/10.1126/science.1128908>

Authors and Affiliations

Imran Nadeem^{1,2}  · Nebojsa Nakicenovic³ · Asma Yaqub¹ · Boris Sakschewski⁴ · Sina Loriani⁴ · Govindasamy Bala⁵ · Thejna Tharammal⁶ · Caroline Zimm³

✉ Imran Nadeem
imran.nadeem@boku.ac.at

Nebojsa Nakicenovic
naki@iiasa.ac.at

Asma Yaqub
asma.yaqub@boku.ac.at

Boris Sakschewski
borissa@pik-potsdam.de

Sina Loriani
sina.loriani@pik-potsdam.de

Govindasamy Bala
gbala@iisc.ac.in

Thejna Tharammal
thejnat@iisc.ac.in

Caroline Zimm
zimmc@iiasa.ac.at

¹ Department of Ecosystem Management, Climate and Biodiversity, Institute of Meteorology and Climatology, BOKU University, Vienna, Austria

² International Water Management Institute, Lahore, Pakistan

³ International Institute for Applied Systems Analysis, Laxenburg, Austria

⁴ FutureLab Earth Resilience in the Anthropocene, Potsdam Institute for Climate Impact Research (PIK), Member of the Leibniz Association, Potsdam, Germany

⁵ Centre for Atmospheric and Oceanic Sciences, Indian Institute of Science, Bangalore, India

⁶ Interdisciplinary Centre for Water Research (ICWaR), Indian Institute of Sciences, Bangalore, India